NOAA Technical Memorandum NWS TDL 77

THE MOISTURE MODEL FOR THE LOCAL AFOS MOS PROGRAM

Techniques Development Laboratory
Silver Spring, MD

December 1985

U.S. DEPARTMENT OF COMMERCE / National Oceanic and Atmospheric Administration / National Weather Service

NOAA Technical Memorandum NWS TDL 77

THE MOISTURE MODEL FOR THE LOCAL AFOS MOS PROGRAM

Techniques Development Laboratory
Silver Spring, MD

December 1985

U.S. DEPARTMENT OF COMMERCE / National Oceanic and Atmospheric Administration / National Weather Service

NOAA TECHNICAL MEMORANDUMS

National Weather Service, Techniques Development Laboratory Series

The primary purpose of the Techniques Development Laboratory of the Office of Systems Development is to translate increases of basic knowledge in meteorology and allied disciplines into improved operating techniques and procedures. To achieve this goal, the Laboratory conducts applied research and development aimed at the improvement of diagnostic and prognostic methods for producing weather information. The Laboratory performs studies both for the general improvement of prediction methodology used in the National Meteorological Service and for the more effective utilization of weather forecasts by the ultimate user.

NOAA Technical Memorandums in the National Weather Service Techniques Development Laboratory series facilitate rapid distribution of material that may be preliminary in nature and which may be published formally elsewhere at a later date. Publications 1 through 5 are in the former series Weather Bureau Technical Notes (TN), Techniques Development Laboratory (TDL) Reports; publications 6 through 36 are in the former series ESSA Technical Memorandums, Weather Bureau Technical Memorandum, (WBTM). Beginning with TDL 37, publications are now part of the series NOAA Technical Memorandums, National Weather Service (NWS).

Publications listed below are available from the National Technical Information Service, U.S. Department of Commerce, Sills Bldg., 5285 Port Royal Road, Springfield, VA 22161. Prices on request. Order by accession number (given in parentheses).

ESSA Technical Memorandums

WBTM TDL 17 Second Interim Report on Sea and Swell Forecasting. N. A. Pore and W. S. Richardson, January 1969, 7 pp. plus 10 figures. (PB-182-273)

WBTM TDL 18 Conditional Probabilities of Precipitation Amounts in the Conterminous United States. Donald L. Jorgensen, William H. Klein, and Charles F. Roberts, March 1969, 89 pp. (PB-183-144)

WBTM TDL 19 An Operationally Oriented Small-Scale 500-Millibar Height Analysis Program. Harry R. Glahn and George W. Hollenbaugh, March 1969, 17 pp. (PB-184-111)

WBTM TDL 20 A Comparison of Two Methods of Reducing Truncation Error. Robert J. Bermowitz, May 1969, 7 pp. (PB-184-741)

WBTM TDL 21 Automatic Decoding of Hourly Weather Reports. George W. Hollenbaugh, Harry R. Glahn, and Dale A. Lowry, July 1969, 27 pp. (PB-185-806)

WBTM TDL 22 An Operationally Oriented Objective Analysis Program. Harry R. Glahn, George W. Hollenbaugh, and Dale A. Lowry, July 1969, 20 pp. (PB-186-129)

WBTM TDL 23 An Operational Subsynoptic Advection Model. Harry R. Glahn, Dale A. Lowry, and George W. Hollenbaugh, July 1969, 26 pp. (PB-186-389)

WBTM TDL 24 A Lake Erie Storm Surge Forecasting Technique. William S. Richardson and N. Arthur Pore, August 1969, 23 pp. (PB-185-778)

WBTM TDL 25 Charts Giving Station Precipitation in the Plateau States From 850- and 500-Millibar Lows During Winter. August F. Korte, Donald L. Jorgensen, and William H. Klein, September 1969, 9 pp. plus appendixes A and B. (PB-187-476)

WBTM TDL 26 Computer Forecasts of Maximum and Minimum Surface Temperatures. William H. Klein, Frank Lewis, and George P. Casely, October 1969, 27 pp. plus appendix. (PB-189-105)

WBTM TDL 27 An Operational Method for Objectively Forecasting Probability of Precipitation. Harry R. Glahn and Dale A. Lowry, October 1969, 24 pp. (PB-188-660)

WBTM TDL 28 Techniques for Forecasting Low Water Occurrence at Baltimore and Norfolk. James M. McClelland, March 1970, 34 pp. (PB-191-744)

WBTM TDL 29 A Method for Predicting Surface Winds. Harry R. Glahn, March 1970, 18 pp. (PB-191-745)

WBTM TDL 30 Summary of Selected Reference Material on the Oceanographic Phenomena of Tides, Storm Surges, Waves, and Breakers. N. Arthur Pore, May 1970, 103 pp. (PB-193-449)

WBTM TDL 31 Persistence of Precipitation at 108 Cities in the Conterminous United States. Donald L. Jorgensen and William H. Klein, May 1970, 84 pp. (PB-193-599)

WBTM TDL 32 Computer-Produced Worded Forecasts. Harry R. Glahn, June 1970, 8 pp. (PB-194-262)

WBTM TDL 33 Calculation of Precipitable Water. L. P. Harrison, June 1970, 61 pp. (PB-193-600)

WBTM TDL 34 An Objective Method for Forecasting Winds Over Lake Erie and Lake Ontario. Celso S. Barrientos. August 1970, 20 pp. (PB-194-586)

WBTM TDL 35 Probabilistic Prediction in Meteorology; a Bibliography. Allan H. Murphy and Roger A. Allen, June 1970, 60 pp. (PB-194-415)

WBTM TDL 36 Current High Altitude Observations--Investigation and Possible Improvement. M. A. Alaka and R. C. Elvander, July 1970, 24 pp. (COM-71-00003)

NWS TDL 37 Prediction of Surface Dew Point Temperatures. R. C. Elvander, February 1971, 40 pp. (COM-71-00253)

NWS TDL 38 Objectively Computed Surface Diagnostic Fields. Robert J. Bermowitz, February 1971, 23 pp. (COM-71-0301)

NWS TDL 39 Computer Prediction of Precipitation Probability for 108 Cities in the United States. William H. Klein, February 1971, 32 pp. (COM-71-00249)

NWS TDL 40 Wave Climatology for the Great Lakes. N. A. Pore, J. M. McClelland, C. S. Barrientos, and W. E. Kennedy, February 1971, 61 pp. (COM-71-00368)

NWS TDL 41 Twice-Daily Mean Heights in the Troposphere Over North America and Vicinity. August F. Korte, June 1971, 31 pp. (COM-71-0286)

(Continued on inside back cover)

NOAA Technical Memorandum NWS TDL 77

THE MOISTURE MODEL FOR THE LOCAL AFOS MOS PROGRAM

David A. Unger

Techniques Development Laboratory
Silver Spring, Maryland

December 1985

UNITED STATES DEPARTMENT OF COMMERCE
Malcolm Balridge, Secretary

National Oceanic and Atmospheric Administration
Anthony J. Calio
Administrator

National Weather Service
Richard E. Hallgren
Assistant Administrator

Table of Contents

THE MOISTURE MODEL FOR THE LOCAL AFOS MOS PROGRAM

ABSTRACT

The moisture model used for the Local AFOS MOS Program (LAMP) is described in this paper. The model predicts the degree of saturation in the single layer between 1000 and 500 mb by a moisture parameter known as the saturation deficit. Moisture is advected under the assumption that no evaporation or condensation occurs along the trajectory. The thickness and elevation of the advected air column determine the degree of saturation. Precipitation is forecast when the air column is saturated.

The model forecasts for instantaneous precipitation were compared to those of persistence and advection of initial precipitation. Model forecasts for three initial times and for both the cool and warm seasons were tested. Results indicated that the moisture model was the most skillful of the three models after 4 hours for cool season predictions, and after 3 hours in the warm season.

A comparison of the forecasts for the occurrence of measurable precipitation in 6-h periods from the LAMP moisture model with those from the LFM model initialized 8 and 13 hours earlier was also made. The LAMP model precipitation forecasts were better than those of the LFM for approximately 10 hours for all initial times and seasons.

An example prediction is shown to illustrate the characteristics of the predictions from the LAMP model.

1. INTRODUCTION

The Local AFOS MOS Program (LAMP) is a system under development at the Techniques Development Laboratory (TDL) which will provide short-range guidance update forecasts on AFOS or similar equipment (Glahn, 1980). LAMP will consist of a series of programs to produce forecasts with model output statistics (MOS) based on locally run numerical models, the most recent hourly surface observations, radar data, and MOS forecasts from the central facility at the National Meteorological Center (NMC). LAMP forecasts will be produced under control of field office personnel.

Centrally-produced MOS guidance products are currently based on numerical models initialized at either 0000 or 1200 GMT and surface observations from 3 hours later. These products are not available until at least 4 hours after the model initialization times. This means the most recent MOS guidance available to a forecaster may be based on data up to 12 hours old. LAMP-based products will make use of the very latest observations and data from simple numerical models which can be initialized and run locally at any time to update MOS guidance.

There are three numerical models used in LAMP: a sea-level pressure (SLP) model (Unger, 1982), an advection model (Grayson and Bermowitz, 1974), and a moisture model. These simple models can easily be run on today's minicomputers

when provided with the proper initial data. The models need hourly forecasts of 500-mb height, which can be obtained from a large-scale numerical model, such as the Limited-area Fine Mesh (LFM) model (Gerrity, 1977; Newell and Deaven, 1981), and surface observations. The LAMP models will be run locally to minimize the amount of data transmitted over the communication network, and to enable the forecaster to examine the model predictions or initial data used in LAMP equations.

A large amount of model output is needed to derive MOS regression equations to predict weather elements. The data required to initialize the LAMP numerical models are available on TDL's archival database for the period from October 1977 through the present. This allows a series of historical predictions to be generated for the derivation of equations. Forecasts from the four year period from October 1977 through September 1981 will be used as dependent data to derive LAMP equations. A fifth season of data will be used for verification of results on independent data. Eventually, all 5 years or more of data will be used to develop the equations to be used in operations. The LAMP predictions will be tested for three initial times, 0800, 1300, and 2000 GMT, which correspond to the times of the latest data available for the morning public forecast, late morning public update, and afternoon public forecast, respectively, issued by forecast office personnel. In addition, guidance from each of these times will support one of the three aviation terminal forecasts. The models will be run over the entire United States on NOAA's mainframe computers to generate historical forecasts. Once the equations are developed, they, like the numerical models, will be run locally.

This paper describes the moisture model used for LAMP. A general review of the principles behind the moisture model is presented, followed by a discussion of the changes that were required to adapt it to LAMP. The precipitation predictions from this model are compared to those from persistence, pure advection, and the LFM model to help determine how effectively the LAMP models use the more recent initial data for short-range prediction.

2. PRINCIPLES OF OPERATION

The LAMP moisture model is patterned after a model run operationally at NMC in the late 1960's known as the SLYH model, named from the last initials of its developers, Sanders, LaRue, Younkin, and Hovermale (Younkin et al., 1965). This moisture model was used as part of the Sub-synoptic Advection Model (SAM) in the early 1970's (Glahn and Lowry, 1972). It is a simple, one-layer numerical model that predicts the degree of saturation between 1000 and 500 mb. The degree of saturation is represented by the saturation deficit, S_d, defined as the amount that the actual 1000-500 mb thickness would have to decrease in order for precipitation to begin for a given amount of moisture present in that column. This quantity can be regarded as the difference between the actual 1000-500 mb thickness (h) and a quantity known as the saturation thickness, (h_s), defined as the thickness at which precipitation would be expected to begin for a given amount of moisture in the column,

$$S_d = h - h_s. \qquad (1)$$

The definition of h_s used here differs slightly from that used in the SLYH model (Younkin et al., 1965), and as originally defined by Swayne (1956), in order to relate S_d more closely to precipitation.

The SLYH model's forecasts are based upon the assumption that atmospheric moisture can be described by a moisture continuity equation shown in Eq. (2).

$$\frac{\partial q}{\partial t} = - \vec{V} \cdot \vec{\nabla} q - \omega \frac{\partial q}{\partial p} \tag{2}$$

Here, q is the specific humidity. $\vec{V}$ is the horizontal advecting wind and ω is the vertical velocity.

The precipitable water, W, can be related to the specific humidity by the following relationship.

$$W = \frac{1}{g} \int_0^{P_1} q \, dp \tag{3}$$

Here P_1 denotes the pressure at the surface and g is the acceleration due to gravity.

By differentiation of Eq. (3) with respect to time and substitution from Eq. (2), an equation for the local change of W with respect to time can be obtained. Through use of climatological approximations to avoid vertical integration, W can be related to S_d and h to find an equation to predict the local rate of change of S_d with time. Details of this derivation can be found in Younkin et al. (1965).

The prediction equation for S_d obtained from the above procedure and expressed in a quasi-Lagrangian framework is:

$$(S_d - 2h + PMA)^{fd} = (S_d - 2h + PMA)^{iu}, \tag{4}$$

where PMA is a terrain term. The superscript "fd" denotes that a term is to be evaluated at the end of a timestep at the downstream end of a trajectory which follows the mean moisture advection in the layer between 1000 and 500 mb (fd = final downstream). The superscript "iu" refers to a quantity which is to be evaluated at the upstream end of that same trajectory at the start of the timestep (iu = initial upstream).

The moisture model conserves a quantity defined by $(S_d - 2h + PMA)$. The S_d changes in response to forecast changes in h and to changes in terrain elevation along a trajectory so that the conservative quantity remains constant.

To help describe the characteristics of the moisture model, Eq. (4) can be rewritten as shown in Eq. (5).

$$\underset{\text{term a}}{S_d^{fd}} = \underset{\text{term a}}{S_d^{iu}} - \underset{\text{term b}}{2(h^{iu} - h^{fd})} + \underset{\text{term c}}{(PMA^{iu} - PMA^{fd})}. \tag{5}$$

The S_d forecast is influenced by three different mechanisms: advection (term a), changes in thickness along the trajectory (term b), and changes in terrain along the trajectory (term c). Together, terms b and c constitute the development terms, so named because they change S_d independently of the initial S_d field.

Trajectories follow an advecting wind, $\vec{V}_E$, formed from a combination of the 1000 and 500 mb geostrophic wind, $\vec{V}_{10}$ and $\vec{V}_5$, respectively, as shown in Eq. (6).

$$\vec{V}_E = .5\ \vec{V}_{10} + .33\ \vec{V}_5. \tag{6}$$

The weightings were determined empirically.

The terrain term in Eq. (5) represents a combination of two effects, that of elevation on saturation thickness, and the effect of changes of elevation on the divergence, and hence on the vertical motion. The functional approximation of the terrain term calculated by Younkin et al. (1965) is given by

$$PMA = .8(1000 - P_G), \tag{7}$$

where P_G is the mean atmospheric pressure in millibars at the model terrain height.

3. INITIAL S_d FIELD

Considerable effort has been devoted to the method of estimation of the initial saturation deficit. Upper air observations, available only at 0000 and 1200 GMT, cannot be used to help initialize the LAMP models directly, since the models may be initialized at any hour. The initial S_d field has to be estimated from available information such as surface observations and recent forecasts of upper air variables from other numerical models.

An earlier study determined that h_s was linearly related to ln(W) and the station elevation, E (Lowry, 1972); data from the eastern two-thirds of the United States were used for this study. Ln(W) was estimated from surface observations so that S_d could be calculated from surface data and an estimate of the thickness (Lowry and Glahn, 1969).

In the current work, the relationship between ln(W), h, and E was re-examined to include data from the entire United States. In addition, a more objective procedure was used to determine the functional relationship between h_s, ln(W), and E. In work described in detail by Lewis et al. (1985), radiosonde observations were categorized by ln(W), h, and E. A value for h_s was selected for each category of ln(W) and E such that the actual thickness was less than the chosen value as often as precipitation was observed for that category. In this way, if a categorical forecast of precipitation were made each time that the observed thickness was less than h_s, precipitation would be forecast as often as it was observed. A regression relationship was developed to relate the values of h_s to the average ln(W) and E for each category. This relationship is shown in Eq. (8).

$$h_s = 5296 + 267\ \ln(W) + .1056\ E \tag{8}$$

Here E is the station elevation. Both E and h_s are measured in meters and W in centimeters.

To estimate ln(W) at stations and times for which upper air observations were not available, a regression equation was developed to relate ln(W) to surface observations and forecasts from the LFM model. Of the many predictors screened,

only the forecast of ln(W) from the LFM, interpolated to the station, and the surface dew point from the station hourly observation were significant. The ln(W), calculated from upper air observations at either 0000 or 1200 GMT, was related to surface observations and the 12-h forecast of ln(W) from the LFM verifying at those times. Separate equations were developed for 0000 and 1200 GMT valid for all stations and seasons in the United States.

The relationships for 0000 and 1200 GMT are shown in Eqs. (9a) and (9b), respectively.

$$\ln(W) = -.3612 + .5920 \ln(\hat{W}) + .01388\ T_d \tag{9a}$$

$$\ln(W) = -.2970 + .6293 \ln(\hat{W}) + .01121\ T_d \tag{9b}$$

T_d is the station observation of dew point temperature in °F, and $\hat{W}$ refers to the 12-h forecast of precipitable water from the LFM in centimeters. The 1200 GMT equation will be used to estimate ln(W) for any hour between 0700 and 1800 GMT; the 0000 GMT relationship will be used at other times.

Eqs. (1), (8), and (9) are used to estimate the S_d at stations where no precipitation is occurring at the observation time. By definition, the S_d is zero at stations where precipitation is occurring. Where the estimated S_d is less than zero and no precipitation is reported, the value of S_d is set to 10 m. The saturation deficit is scaled before entry into an objective analysis program. Scaling is necessary because of an inherent difficulty in the interpolation of an S_d field (objective analysis is merely an interpolation of irregularly spaced observations to a evenly spaced grid). An interpolation usually assigns a value to a point based on a weighted combination of the surrounding data. Since S_d is set precisely to zero where precipitation occurs, if one or more surrounding points have a positive value, the interpolated value will nearly always be positive. This will greatly reduce the apparent area of precipitation if only points where $S_d = 0$ denote precipitation. Values are scaled to allow a precipitation observation to have a greater influence on surrounding gridpoints. A negative S_d is temporarily assigned to stations which report precipitation. Positive values are reduced to lessen the discontinuity at the zero line. A Cressman type successive correction analysis is then used to obtain S_d on the LAMP grid (see Glahn et al., 1985).

The variable is analyzed over the area shown in Fig. 1. The grid is on a polar stereographic projection with grid spacing of about 95 km at 60°N. The grid spacing is shown in the lower left corner of the figure. After the analysis, any gridpoint with a negative S_d is set to zero, and gridpoints with positive values are rescaled to restore the field.

Manually Digitized Radar (MDR) data, when available, are used to further define the S_d in areas near radar returns. Radar data are collected each hour by the National Weather Service and saved on a 47-km grid, one-half the mesh length used in LAMP (Foster and Reap, 1978). The maximum echo intensity within a box centered over each MDR gridpoint is reported at 35 minutes past each hour. The LAMP model gridpoints are aligned with the corners of these MDR boxes such that each MDR block forms a quadrant of a larger square centered at the LAMP gridpoints. The relationship between the LAMP gridpoints, represented by the circles, and the MDR blocks is illustrated in Fig. 2. The gridpoint at Q is the center of a box defined by the four MDR blocks labeled A through D.

The S_d is reduced by the percentage of the four surrounding MDR squares with echos of any intensity from the most recent radar observation (taken 25 minutes before the hour). If radar returns were reported in 3 of the 4 surrounding MDR boxes, for example, the S_d for that gridpoint would be reduced by 75%. Since radar echoes can result from precipitation not reaching the ground, and because the percent coverage within any 47-km grid square is not available, the S_d is never reduced to a value less than 5 m on the basis of an MDR report alone. The S_d will be reduced to 5 m at gridpoints where MDR echos are reported in all surrounding MDR blocks. Gridpoints where the S_d's are initially analyzed to be less than 5 m are unaffected by MDR reports. In this way, the analysis will indicate precipitation only where surface reports of precipitation have been received. Details of the analysis procedure are discussed in Glahn et al. (1985).

4. PREDICTION PROCEDURE

The model uses a quasi-Lagrangian integration technique to forecast S_d each hour through 22 hours. One hour forecast trajectories which end over gridpoints are calculated from the 500- and 1000-mb heights provided hourly from the LFM and the LAMP SLP models. The trajectories are formed by an iterative technique that uses two half-hour trajectories computed from the geostrophic winds formed from the geopotential height forecasts from both the start and end of the 1-h timestep.

Terms in Eq. (5) are interpolated to the trajectory origins to obtain the values marked "iu". These values are then used as the "fd" values at the gridpoints at the downstream ends of the trajectories. The forecast S_d is then used on the next timestep.

A special interpolation procedure to preserve precipitation areas is used on the S_d field. The model uses linear interpolation between gridpoints to obtain its initial upstream values. The broken line in Fig. 3 illustrates, in one dimension, how a linear interpolation will distort the precipitation area represented by $S_d = 0$. The linear interpolation will indicate precipitation only over the single point, directly over the gridpoint labeled "2". The interpolation was modified to place the zero line about half way between a gridpoint with $S_d = 0$ and one with a positive value, regardless of its magnitude, as illustrated by the solid line in Fig. 3. The modified interpolation will indicate precipitation ($S_d = 0$) everywhere between the points marked by the arrows. The modified interpolation procedure is discussed in the Appendix.

5. PRECIPITATION PREDICTIONS

When an initially low S_d is forecast to decrease, it can become negative, which indicates that the amount of moisture present in the 1000-500 mb layer is in excess of that expected to produce precipitation. Since the model does not allow for condensation, we remove excess moisture at the end of a timestep by adjusting any negative S_d gridpoint value to 0. In theory, the amount of this adjustment is proportional to the precipitation amount in the given timestep. The amount of the adjustment can be accumulated at a particular gridpoint to represent the total precipitation in a time interval. We define a quantity known as the accumulation of adjustment of S_d (AS_d) to be the sum of the negative S_d's within a time period at any given gridpoint. The AS_d is set to zero when the S_d is zero on one or more timesteps but is never

negative within the interval. When the S_d remains positive throughout the time period, the AS_d is assigned the average of the S_d values at the end of each timestep within the interval.

The moisture model forecasts of S_d for each hour are saved to magnetic tape for derivation and testing of LAMP forecast equations. When the moisture model predicts the S_d to be negative at the end of a timestep, that value is saved as a 1-h AS_d for that gridpoint. The 6-h AS_d's for periods ending at 0000, 0600, 1200 ,and 1800 GMT and the 12-h AS_d's for periods ending at 0000 and 1200 GMT are also saved. AS_d's for periods shorter than 6 or 12 hours are stored in place of the 6- or 12-h AS_d's when the first occurrence of the aforementioned times is before the 6- or 12-h projection, respectively, in which case the accumulations are from the initial time.

6. TUNING AND VERIFICATION PROCEDURES

We extensively tested the moisture model over the conterminous United States. The moisture model is an advective model which conserves the mean moisture content along a trajectory except when the prediction equation indicates saturation. There, the moisture is removed as precipitation by an adjustment to the S_d. We evaluated the moisture model primarily on the basis of its precipitation forecasts.

The 1-h AS_d's were used to forecast the occurrence of precipitation at times corresponding to the station hourly observations for projections of from 1 to 20 hours. Precipitation was forecast each time $S_d \leq = 0$ when interpolated to a station location.

The S_d's or AS_d's are interpolated to specific station locations by an interpolation routine similar to that used to find the upstream S_d values in the moisture model. Note that for forecast S_d fields, both negative and positive values occur, since 1-h AS_d's are stored in place of zero S_d's. The interpolation routine will place the zero line approximately halfway between gridpoints of alternate signs, regardless of the magnitude of the value at either gridpoint, with a linear transition from the value at the gridpoint on either side of the line to zero. The position of the zero line will be nearly the same as it would be if the AS_d's were replaced with zeros, therefore, the interpolation routine actually behaves as if it were making two interpolations, one for the S_d (positive) values, and one for the AS_d (negative) values, with the fields forced to match at the zero line. Detail of this interpolation procedure is presented in the Appendix.

The precipitation forecasts were evaluated with the Critical Success Index (CSI) (Donaldson, et al., 1975), also known as the Threat Score. This score measures the ratio of the number of correctly forecast events to the number of events that were either forecast or actually occurred. For the current study, the stations were evenly distributed so the score is approximately equivalent to the ratio of the area of correct precipitation forecasts to the area over which precipitation was either forecast or actually occurred. A perfect forecast would have a CSI of 1 and a prediction for which not a single hit was scored would have a CSI of 0.

The bias was also used to evaluate the forecasts. It measures the ratio of the total forecasted events to the total number of observed events. Again, for

this study, it can be regarded as the ratio of the predicted to the observed area of precipitation.

In equation form, these scores can be expressed by

$$CSI = \frac{H}{F + O - H} \qquad \text{and}$$

$$BIAS = \frac{F}{O},$$

where F is the total number of forecast events, O is the number of observed events, and H is the total number of correctly forecast events (hits). In our study, an event is the occurrence of precipitation.

The bias of a set of forecasts, ideally, should be close to 1; however, on categorical forecasts of variables with a low frequency of occurrence, slightly inflated biases are of little concern since the actual number of forecasted events which did not occur in that case would be relatively low. Since the bias is a ratio, biases of .5 and 2 may be considered equally skillful for some applications, even though the algebraic distance between the two scores and 1 is different by a factor of two.

7. MODEL REVISIONS

Tests on the moisture model revealed there was a sharp drop in the number of gridpoints with $S_d \leq 0$ in the first timestep. This represented a large decrease in the area of precipitation forecast by the model and apparently occurred because initial precipitation often existed in areas where the S_d tendency from the development terms in Eq. (5) was positive. Any increase in S_d in an area of initial precipitation, regardless of its magnitude, will end the precipitation in that timestep. Verification indicated this was unrealistic.

We decided to emphasize the advection terms in areas of initial precipitation in the early projections to help improve the moisture model's handling of precipitation. The development terms of the model are partly based upon 500-mb height forecasts from a large scale model, which could be up to 14 hours old, as well as on a considerably smoothed terrain term. In addition, some precipitation areas exist due to mechanisms not handled by the simple model physics (convective precipitation, for example). If eliminated by the model's development terms, much of the initial information provided from the precipitation field will be lost.

To help retain some areas of precipitation, the development terms (terms b and c in Eq. (5)) are ignored in areas of precipitation if, together, they are positive, but below a certain threshold magnitude. The threshold was chosen such that the area of precipitation remained approximately the same in the early timesteps. If the tendency exceeds the threshold, the S_d is assigned the value of the excess which was forecasted. Note that this applies only to the development terms in the equation, not to advection (the moisture model actually forecasts the S_d in two steps: first the S_d field is advected, then the development terms are computed and added).

The threshold value is reduced fractionally on each succeeding timestep until it is eliminated after the tenth timestep. The initial magnitude of the

threshold is 7 m and this value is reduced by .7 on each timestep. This procedure is used on the first ten timesteps, after which the threshold is set to zero and the moisture model is returned to its original formulation.

8. RESULTS

A. Forecasts of Instantaneous Precipitation

The moisture model forecasts were tested for both the cool and the warm seasons. Twenty-one cases were chosen from January through March of 1979 to evaluate cool season predictions. An additional 21 cases from the months of July through September 1979 were used to test warm season forecasts. Cases were from approximately every third day in the tested periods. Predictions from model runs initialized at 0800 and 1300 GMT were tested for both seasons. In addition, the 2000 GMT initial time was tested for the warm season predictions. Categorical precipitation forecasts for 216 stations, evenly distributed throughout the United States, were made from the 1-h AS_d forecasts. This yielded approximately 4300 forecasts on each projection for each sample.

The predictions were compared to precipitation forecasts made from persistence and those from an even simpler advection model. The advection forecasts were obtained from a LAMP moisture model in which the thickness and terrain terms (terms b and c in Eq. (5)) were neglected. The forecast equation for this model is then,

$$S_d^{fd} = S_d^{iu}.$$

Precipitation was forecast at a particular station when $S_d = 0$. An interpolation similar to that used for the moisture model forecasts was used for the advection predictions.

The persistence forecasts were made for each station from which an observation of the present weather was available at the initial time. Since a persistence forecast was not available at all stations, because of missing initial observations, while model forecasts were available at all stations, the forecasts from persistence and the models were not exactly matched. This occasionally results in minor discrepancies when the biases of the forecasts are examined.

Fig. 4 shows results from the cool season predictions from forecasts initialized at 0800 GMT. The advection and persistence scores are nearly the same for the entire sample of forecasts even though considerable variation occurred on individual cases.

The moisture model forecasts are initially worse than either persistence or advection; however, after the first timestep the CSI for the moisture model decreases more slowly than the other forecasts. At about 5 hours, the CSI's for the three models are about the same, after which the LAMP model scores highest.

The bias of the moisture model increases steadily throughout the forecast. By the 22-h projection, the bias for the moisture model is about 40% over persistence which, of course, has a constant number of precipitation forecasts for all projections. The frequency of precipitation for this sample is about 20% initially, and decreases to about 16% in the later projections.

Results from forecasts initialized at 1300 GMT (not shown) are very similar to those from 0800 GMT. The 500-mb heights used for this start time are from the 0000 GMT LFM model run. These are identical to those used by the 0800 GMT LAMP model runs to make the forecasts past 1300 GMT. The dew points, sea level pressure, and the observed weather are taken from 1300 GMT observations. The MDR data used for this initial time are also more recent, taken at 1235 GMT. The LAMP SLP model is initialized by the 1300 GMT sea level pressure reports; therefore, the 1000-mb heights used for this initial time are from a more recent forecast than those used for the 0800 GMT moisture model forecasts.

A comparison between persistence and moisture model forecasts initialized at both 0800 and 1300 GMT is shown in Fig. 5. Projections displayed are from 0800 GMT; the 1300 runs begin at the 5-h projection from 0800 GMT.

The scores for the LAMP models initialized at 1300 GMT were consistently higher than model runs initialized 5 hours earlier (0800 GMT) for about 15 hours (through 0400 GMT), although there was very little difference in scores past 7 hours (2000 GMT). Persistence forecasts from 1300 GMT, on the other hand average considerably higher than those from 0800 GMT through at least 0600 GMT the next day, a 17-h projection.

The biases for the moisture model runs initialized at 0800 and 1300 GMT rapidly approach the same level, while those from persistence maintain approximately the same ratio throughout the forecast period.

Fig. 6 shows the results for warm season predictions from 0800 GMT. The skill of the forecasts in this season are well below those obtained in the winter. As for the cool season, advection and persistence are about equally skillful for every projection. The CSI for the moisture model, initially about the same as both persistence and advection, becomes higher than for the other two forecasts after the 3-h projection. Beyond 12 hours, the skill of the forecasts remains about constant, with a CSI for the moisture model of about .11, .05 for persistence, and .07 for advection.

The biases for persistence show the effect of the diurnal cycle in precipitation frequency for the warm season, with the development of a dry bias the result of higher precipitation frequency in the afternoon (projections from 10 to 20 hours). The advection forecasts show a slight tendency to increase the area of precipitation as the forecasts progress, as indicated by the increase in bias in relation to persistence forecasts. This may be partly an effect of the special interpolation procedure. The biases for the moisture model increase at a rate somewhat higher than for advection.

Results from 1300 GMT (not shown) are very similar to those from 0800 GMT in the warm season. The CSI decreases--rapidly at first, then more gradually--until it becomes stable after the 12-h projection. The bias is primarily influenced by the diurnal cycle in the precipitation frequency. The model biases are low in the afternoon hours and then increase sharply after the 13-h projection (0400 GMT).

At 2000 GMT (Fig. 7), the forecasts behave somewhat differently since they are initialized at a time of active convection. The forecasts are significantly less skillful than those from the morning hours, with the CSI for a 1-h projection of about .3. The CSI for the moisture model is only slightly above

persistence and advection in skill until about 0400 GMT (an 8-h projection). Past this hour, the CSI increases slightly for the moisture model forecasts while the persistence and advection scores continue to fall for another two hours.

The bias of the forecasts at 2000 GMT are dramatically different from other hours in the warm season since the forecasts are initialized during a period of active convection. As the precipitation frequency decreases in the evening hours, the persistence forecasts develop a high bias; the bias of the advection model forecasts become considerably higher than that of the persistence forecasts. The bias from the moisture model also becomes quite high and is higher than that for the advection model, which indicates that the development terms contribute to the increase in the amount of precipitation.

A comparison between the scores generated by the model forecasts from 1300 and 2000 GMT is shown in Fig. 8. Moisture model scores for both initial times become about the same after the 7-h projection from the more recent model run, although the scores of the latter remain very slightly higher throughout the period of comparison. The CSI's for persistence forecasts initialized at 2000 GMT also become nearly the same as those from 1300 GMT after the 7-h projection.

Results from a comparison between 0800 and 1300 GMT (not shown) are similar except that the scores from the model initialized at 1300 GMT are better than those from 0800 GMT for about 12 hours.

B. Forecasts of Measurable Precipitation in 6-h Periods

The forecasts from the moisture model were compared to those from the most recently available LFM in order to estimate the value of the more timely but less sophisticated LAMP moisture model. The more detailed and recent initial field which is used to initialize the moisture model provides more accurate forecasts for the initial projections; however, at longer projections, the simple model physics of the moisture model results in less accurate forecasts than from the LFM. The length of time for which the LAMP model provides more accurate forecasts determines its effectiveness to update guidance based on the LFM.

One important aspect of the predictions not measured by the comparisons presented here is the value to the field offices of receiving LAMP forecasts more frequently. Forecasts from the LFM model are available only every 6 hours; the large amount of resources required to prepare the output and to transmit the forecasts prevents more frequent output. The LAMP moisture model will be run on station to provide hourly forecasts. The information provided by hourly output is valuable for the timing of moisture-related predictions and cannot be measured at this time by comparisons between the models.

Forecasts for measurable precipitation within 6-h periods were made from the 6-h AS_d forecasts for the same 216 stations and for the same sample used for the hourly forecasts. Verifying observations were from the 6-h precipitation amounts which are reported in the hourly surface observations at 0000, 0600, 1200, and 1800 GMT. A categorical precipitation forecast was made each time the 6-h AS_d, interpolated to stations, was zero or negative. The verifying observation was the occurrence of a precipitation amount greater than or equal

to .01 in. For LFM model forecasts, measurable precipitation was predicted when precipitation amounts, interpolated to the station, were greater than .2 mm. These interpolations were also done with a routine designed to place the zero line about halfway between gridpoints with precipitation and those with no precipitation.

For the 0800 and 1300 GMT initial times, the most recent LFM model available to the forecaster would be from 0000 GMT. The most recent LFM forecasts available at 2000 GMT would be from 1200 GMT. At 0800 and 2000 GMT, the LAMP model run is based on data which are 8 hours more recent than the most recent LFM model. The LAMP predictions for the 4-, 10-, 16-, and 22-h projections correspond to the 12-, 18-, 24-, and 30-h projections, respectively, from the LFM model. The 18-, 24-, and 30-h projections from the LFM model similarly correspond to the 5-, 11-, and 17-h projection for the LAMP models initialized at 1300 GMT.

Results from cool season predictions initialized at 0800 GMT are shown in Fig. 9. The moisture and advection model forecasts for 1200 GMT are from a 4-h AS_d and, therefore, represent an accumulation of precipitation from the initial time. The verifying observation for this projection is the 6-h precipitation amount ending at that time.

The moisture model is slightly worse than advection at this projection, but is substantially better by the next period (the 4-h to 10-h prediction) and beyond. Scores from the LFM model initialized at 0000 GMT are worse than the LAMP model for the 6-h period ending at 1200 GMT (a 4-h LAMP model projection compared to a 12-h LFM model projection). By 1800 GMT, the scores for the 10-h projection from the LAMP moisture model and the LFM 18-h projection are nearly the same. At 0000 GMT, the LFM model predictions are better than those from LAMP.

The bias for the LAMP moisture model increases steadily throughout the forecast at a rate faster than either advection or the LFM model. The frequency for measurable precipitation for this sample falls from about 20% for the 6-h period ending at 1200 GMT to about 17% for the 22-h projection. A prediction which maintains a constant precipitation frequency would have a bias of about 1.2 on the 22-h projection.

At 1300 GMT for the cool season (Fig. 10) the results are much the same. Advection scores are nearly the same as the moisture model at 5 hours, but become rapidly worse after that. The relationship between the LFM and moisture model scores are nearly the same for the LAMP forecasts initialized at 0800 and 1300 GMT, despite of the more recent initial data. This occurs because the LFM's CSI remains nearly constant throughout the four 6-h periods verified, while the LAMP moisture models initialized at the two times behave similarly in relation to their respective initial times. Note that the LFM model initialized at 0000 GMT is still used for comparison because the 1200 GMT run would not normally be available by the time the 1300 GMT moisture model forecasts are complete.

Warm season results for 0800 GMT are shown in Fig. 11. The moisture and advection models show a very low bias for all the 6-h intervals. The low bias in the first period may be due in part to the short accumulation period (a 4-h AS_d is used to forecast 6-h precipitation accumulations). Another contributing

factor is the abundance of convective precipitation in the warm season. The formation and dissipation of convective precipitation may not be represented by the synoptic scale changes in thickness or elevation along a trajectory and, therefore, cannot be adequately handled by the moisture model. The diurnal change in precipitation also cannot be handled. The greater frequency of precipitation in the afternoon will result in a low bias for precipitation on forecasts initialized in the morning hours.

The extent of the model's convective precipitation is governed by the amount of precipitation of that type at the initial time. The moisture model will advect these precipitation areas with the flow, but will not necessarily develop areas of new convection. Since much of the summertime precipitation may be from areas of new convective development, the amount of precipitation is underestimated by the moisture model.

The CSI for 0800 GMT summertime predictions is initially higher than the LFM but rapidly decreases until, at 10 hours, the scores for the LAMP moisture model and the LFM are equal. The moisture model scores continue to decrease rapidly so that the LFM becomes substantially better by the 16-h LAMP projection. Note that the scores for the LFM model increase between 1200 and 0000 GMT. The LFM model greatly overforecast precipitation in the early projections, with a bias of 4.6 for the 6-h period ending at 1200 GMT which resulted in the low CSI for that projection.

Results from forecasts from model runs initialized at 2000 GMT are shown in Fig. 12. The LFM forecasts here are from the model runs initialized at 1200 GMT; therefore, the relationship between the LFM and LAMP model forecast projections are similar to those from 0800 GMT. The LFM model predicts the extent of precipitation to be excessive for the 6 to 12-h projection. This reduces the CSI of the model in this projection. On the later projections, as the bias becomes more reasonable, the LFM's CSI increases slightly.

The moisture model forecasts begin with the characteristically low warm season bias in the early projections, but the bias steadily increases as the forecasts progress. The advection forecasts follow a similar pattern, although they are somewhat drier. The CSI for the moisture model drops sharply in the first two forecast periods to reach its lowest point for the 6-h period ending at 0600 GMT, after which it rises slightly, a reflection of the better bias of the later projections.

The CSI for advection declines steadily throughout the forecast period. The bias of the forecasts increases as the projection increases, but remains lower than the moisture model.

The low bias of the warm season moisture and advection model predictions indicate that the use of 0 as a threshold value for the AS_d to delineate precipitation is too stringent. Much of the precipitation may occur when the moisture model does not predict the atmosphere to be saturated at any timestep within the 6-h period. If precipitation were forecast when the 6-h AS_d was forecast to be less than 30 m, for example, the bias of the forecasts would be about 1 and the CSI would be higher by about .05 for each projection.

The excessive bias of the LFM forecasts in the early projections was similarly controlled for purposes of comparison. The forecast precipitation

amount from the LFM was required to be in excess of a certain value before a categorical precipitation forecast was made for that station. If this value was not exceeded, no precipitation was forecast at the station, regardless of whether or not the LFM forecast a measurable amount of precipitation.

Fig. 13 shows the scores which would result if the threshold value used to delineate precipitation from the moisture and advection model forecasts of AS_d's, or from the precipitation amount forecasts in the case of the LFM, is chosen to maximize the CSI for the sample forecasts. The threshold values for AS_d were usually between 20 and 60 m. Moisture model forecasts were from the 0800 GMT initial time, LFM forecasts were from the 0000 GMT run. The results suggest that the crossover in the CSI is about 16 hours for the 0800 GMT initial time when an adjustment is made for the bias, although the differences between the two model's scores are minor past the 10-h LAMP projection.

The bias-controlled results indicate that the moisture model initialized at 2000 GMT is slightly less skillful than when it is initialized at 0800 or 1300 GMT. The LAMP model forecasts from 2000 GMT are better than those from the LFM initialized 8 hours earlier for about 10 hours. The CSI from the advection model at the 4-h projection is slightly better than the moisture model. This suggests that the LAMP model would make the greatest improvement over the forecasts currently available on projections between 5 and 10 hours at 2000 GMT in the warm season.

C. Example Forecast

The moisture model forecast initialized at 0800 GMT on March 10, 1979 is presented to illustrate the model's characteristics. This case was chosen because of a sharp front located in the eastern United States and associated, well-defined, frontal precipitation. This same case was used in earlier publications to illustrate the LAMP SLP model (Unger, 1982) and the LAMP analysis procedures (Glahn, et al., 1985).

The Daily Weather Map (U.S Department of Commerce, 1979) for 1200 GMT on March 10, 1979, is shown in Fig. 14. A sharp cold front trails from a low pressure system over southern Ontario southward to near the Gulf coast.

The initial saturation deficit at 0800 GMT, four hours previous to the Daily Weather Map time, is shown in Fig. 15. The S_d is contoured at 40-m intervals, with the area where $S_d = 0$, which indicates precipitation, shaded. The frontal precipitation is clearly defined, as is precipitation associated with the low. An area of precipitation associated with an upper-level trough is over the Kansas-Missouri border.

The 12-h forecast of S_d is shown in Fig. 16, with the verifying analysis illustrated in Fig. 17. The moisture model forecast the frontal precipitation in the eastern United States quite well from Georgia northward but moved the leading edge of the precipitation slightly too fast. The dry areas are positioned quite well, but the S_d is too high, which indicates that the moisture model forecasts were too dry.

The forecast over the Gulf Coast states and New Mexico was poor. The moisture model predicted an end to the precipitation and considerable drying from Alabama to eastern Texas, where precipitation was occurring at 2000 GMT. The

precipitation in western Texas and New Mexico was enlarged, but it actually disappeared.

The excessive drying, a problem which is characteristic of the moisture model, originates mostly from the thickness term. The term may overestimate the drying due to subsidence in some active weather situations (the coefficient which multiplies the thickness term would be 1 if the effect of vertical velocity on saturation thickness were eliminated). This may be, in part, because of the SLP model's tendency to overbuild high pressure systems, which increases the thickness and, hence, overestimates drying. In addition, the lack of evaporation in the model undoubtedly contributes to an overestimate of drying.

The moisture model's failure to handle the precipitation along the Gulf coast is most likely due to an underestimate of low level moisture from the Gulf of Mexico.

The precipitation over New Mexico is an example of a problem which can result in the moisture model's representation of precipitation. The precipitation over New Mexico occurred in an area where the S_d estimate, unmodified by the precipitation observations, was quite high. The S_d estimates in this region were overridden and set to zero. This may have contributed to an overestimate of the moisture content in the region.

These errors are examples of problems which can result from the very simple dynamics of the LAMP moisture model. Some cannot be corrected without more upper air information. Since the moisture model is designed to be run locally on minicomputers, and because it is to be an update model, it must be computationally simple and can use only data available at every hour. No changes (other than the persistence correction mentioned earlier) were found to improve the overall performance of the model's precipitation forecasts given these limitations.

An example of a 4 to 10 h forecast of measurable precipitation and the verifying observed precipitation area is shown in Fig. 18. Shaded areas indicate where precipitation was correctly forecast in this 6-h period ending at 1800 GMT on March 10, 1979. The frontal precipitation was predicted quite well in the northeastern United States. The trailing edge of the precipitation is defined sharply by the moisture model, since it is governed by the location of precipitation at the 4-h projection. The area of precipitation in western Texas and New Mexico was forecast by the moisture model. This is likely to be from precipitation early in the period, since the S_d analysis at 2000 GMT indicated precipitation had ended in the region by that time (see Fig. 17). The LAMP moisture model indicated some precipitation over Michigan, but misplaced the location. Precipitation over the Western Gulf coast states was not forecasted.

Fig. 19 shows the relationship between the observed precipitation and the 12- to 18-h precipitation forecast from the LFM model. The LFM model also forecasted the frontal precipitation well; however, the precipitation area was not as sharply defined, especially the western boundary. It missed the precipitation over Texas and New Mexico, and had no indication of precipitation over Michigan. The leading edge of precipitation in the northeastern United States was well forecasted.

Results from this example are consistent with the verification scores since the overall performance of the LFM and moisture model for the 4- to 10-h precipitation forecasts appear quite similar. On close examination, the LAMP model exhibits better forecasts for the earlier part of the period, indicated by the positioning of the trailing edges of precipitation. The trailing edges, in general, are determined by the location of precipitation in the early part of the period, when the accuracy of the updated predictions is greater. By the 10-h projection, LAMP model forecasts are about equal or slightly worse in quality than those from the LFM, as evident from leading edges of precipitation.

9. SUMMARY AND CONCLUSIONS

The LAMP moisture model is a simple numerical model which forecasts saturation in a single layer. The degree of saturation is indicated by the saturation deficit, defined as the amount which the 1000-500 mb thickness would have to decrease in order for precipitation to begin, given the moisture content in that layer. The model predicts the S_d from an estimate of initial S_d, the terrain elevation, and hourly forecasts of thickness provided from other models under the assumption that the moisture is conserved along the trajectory formed by an estimate of the mean moisture transport. Precipitation is represented by a forecast value of S_d of zero or less, with negative S_d values set to zero at the start of each timestep. The adjustment of the negative values to zero represents the removal of moisture from the model, hence, precipitation. Precipitation for periods longer than a single timestep is represented by the accumulated saturation deficit values, AS_d.

The model was revised slightly from the earlier SAM model on which it was based, to increase the accuracy of forecasts in the early projections. Small increases in S_d forecast by the development terms were ignored in areas of precipitation. This procedure effectively emphasized the advection term in the early projections. The emphasis was gradually reduced until the model was returned to its original formulation on the 10-h projection.

Cool season results indicate the moisture model is more skillful than persistence in the prediction of instantaneous precipitation after about 4 hours. Persistence is initially better, but the accuracy of the forecasts decrease rapidly through 22 hours; advection forecasts are about equally skillful as persistence. The moisture model increases the amount of precipitation gradually with time after the elimination of some precipitation in the first timestep.

Warm season results indicate persistence, advection, and the moisture model forecasts of instantaneous precipitation are about equally skillful through 3 hours, after which the moisture model forecasts are more accurate. Advection and persistence remain about equally skillful. The bias of the forecasts depends on the initial time: forecasts initialized in the morning hours underpredict precipitation; those initialized at 2000 GMT overpredict precipitation. The moisture model showed a tendency to increase the extent of precipitation as the forecast progressed.

The results from the comparison of LAMP model forecasts at different initial times indicate that the model loses most of the advantage provided by the more recent initial field after about 10 hours. In the warm season, for example, the CSI becomes nearly constant after 7 or 8 hours.

Forecasts of measurable precipitation in 6-h intervals from the moisture model in the cool season are more accurate than the LFM at the 4-h projection, but not quite as accurate for the 6-h period ending at 10 hours (an 18-h projection for the LFM). At 1300 GMT, the 5-h projection from the moisture model is considerably better than the most recently available LFM forecasts (an 18-h projection); however, by the 11-h projection from 1300 GMT (a 24-h forecast for the LFM), the skill of the moisture model forecasts is slightly lower. Interpolation of the scores suggest a crossover in accuracy at about 10 hours. Advection, although slightly more skillful than the LAMP moisture model at the 4-h projection, rapidly loses its skill as the forecast progresses, with the forecasts much less accurate for projections of 10 hours or greater.

Warm season predictions show similar results for forecasts initialized in the morning; however, the moisture model forecasts severely underestimate the extent of precipitation, while the LFM model greatly overestimates the precipitation area especially for the 12-h projection. The true skill of the models under these circumstances may be better represented by a comparison of scores when the precipitation forecasts are adjusted to account for systematic biases. The moisture model forecasts appear to be more accurate than the LFM for more than 10, but less than 16 hours when an adjustment is made for systematic biases in both models; however, there does not appear to be a great difference in skill between the LFM and LAMP models past 10 hours.

ACKNOWLEDGMENTS

The author gratefully acknowledges the many helpful suggestions provided by Harry R. Glahn. The drafting support provided by Chad E. Myers is also greatly appreciated.

REFERENCES

Donaldson, R., Jr., R. Dyer and M. Kraus, 1975: An objective evaluator of techniques for predicting severe weather events. Preprints Ninth Conference Severe Local Storms, Norman, Amer. Met. Soc., 321-326.

Foster, D. S., and R. M. Reap, 1978: Archiving the new manually digitized radar data. TDL Office Note 78-5, National Weather Service, NOAA, U.S. Department of Commerce, 15 pp.

Gerrity, J. F., Jr., 1977: The LFM model-1976: A documentation. NOAA Technical Memorandum NWS NMC-60, National Oceanic and Atmospheric Administration, U.S. Department of Commerce, 68 pp.

Glahn, H. R., T. L. Chambers, W. H. Richardson, H. P. Perrotti, 1985: Objective map analysis for the Local AFOS MOS Program. NOAA Technical Memorandum NWS TDL-75. National Oceanic and Atmospheric Administration, U.S. Department of Commerce, 34 pp.

_____, 1980: Plans for the development of a Local AFOS MOS Program (LAMP). Preprints Eighth Conference on Weather Forecasting and Analysis, Denver, Amer. Meteor. Soc., 302-305

_____, and D. A. Lowry, 1972: An operational subsynoptic advection model. J. Appl. Meteor., 11, 578-585.

Grayson, T. H. and R. J. Bermowitz, 1974: A subsynoptic update model and forecast system with application to aviation weather. Project Report No. FAA-RD-74-100, U.S. Department of Transportation, Washington D.C. 48 pp.

Lewis, F., D. A. Unger, and J. R. Bocchieri, 1985: Estimation of saturation thickness to initialize the LAMP moisture model. Mon. Wea. Rev. 113, 1933-1941.

Lowry, D. A., 1972: Climatological relationships among precipitable, water, thickness and precipitation. J. Appl. Meteor., 11, 1326-1333.

_____, and H. R. Glahn, 1969: Relationships between integrated atmospheric moisture and surface weather. J. Appl. Meteor., 8, 762-768.

National Weather Service, 1974: Postprocessing the LFM forecasts. Tech. Proc. Bull. No. 174, National Oceanic and Atmospheric Administration, U.S. Department of Commerce, 14 pp.

Newell, J. E., and D. G. Deaven, 1981: The LFM-II model--1980. NOAA Technical Memorandum NWS NMC-66, National Oceanic and Atmospheric Administration, U.S. Department of Commerce, 20 pp.

Swayne, W. W., 1956: Quantitative analysis of forecasting of winter rainfall patterns. Mon. Wea. Rev., 84, 53-65.

Unger, D. A., 1982: The sea level pressure prediction model of the Local AFOS MOS Program. NOAA Technical Memorandum NWS TDL 70, National Oceanic and Atmospheric Administration, U.S. Department of Commerce, 33 pp.

U.S. Department of Commerce, 1979. Daily Weather Maps. U.S. Government Printing Office.

Younkin, R. J., J. A. LaRue, and F. Sanders, 1965: The objective prediction of clouds and precipitation using vertically integrated moisture and adiabatic vertical motions. J. Appl. Meteor., 4, 3-17.

APPENDIX

Special interpolation procedures are required for gridded fields of S_d, AS_d, and precipitation amount because the location of the zero line, which denotes the edge of precipitation areas, is not reasonably placed by conventional (e.g., bilinear) interpolation procedures. These special procedures are used so that the zero line is placed approximately half way between a point with a positive value and an adjacent point with a zero or negative value regardless of the magnitudes of the numbers on either side of the line. The value on either side of the zero line is obtained by linear interpolation.

The procedure for S_d and precipitation amount is as follows. For each gridpoint where $S_d = 0$ and an adjacent gridpoint is positive, the zero value is temporarily replaced with the negative of the positive value. If more than one adjacent point is positive, the magnitude of the temporary negative value is the average of these positive values. For this purpose, each interior gridpoint has four adjacent points, a corner point has two adjacent points, and other boundary points have three adjacent points. A bilinear interpolation is then performed on this new field, with any resulting negative values set to zero.[1]

The algorithm used to interpolate into the AS_d fields, developed especially for the LAMP moisture model by the author, must return negative as well as positive values, with the zero line about midway between gridpoints with alternate signs. This is accomplished by a similar approach to that described above, except that two interpolations are performed. In one, the negative or zero AS_d's are temporarily replaced when any adjacent gridpoints are positive in a way similar to the S_d interpolation. In the other, the positive values which have negative neighbors are replaced in a like fashion except with the signs reversed. Note that zero gridpoint values are regarded as negative for the determination of sign changes between gridpoints.

The final value is determined from the positive interpolation (where the negative values are replaced) in areas where both interpolations indicate that $AS_d \geq 0$. The value from negative interpolation is selected when both interpolations are negative. When a discrepancy exists, the interpolated value is set to zero.

Fig. 20a illustrates this interpolation procedure in one dimension on arbitrarily selected values. There are only minor discrepancies in this example, since the sign of the interpolation for the two positive and negative interpolations agree most of the time.

Fig. 20b illustrates situations where discrepancies exist. The positive interpolation, shown by the dashed line, is meaningful only when it is greater than zero, since it is derived from a field in which the negative values are changed for the placement of the zero line. The negative interpolation, shown by the dotted line, is meaningful only when it is less than zero, since the positive values are altered on the field from which it is computed. Usually

---

[1]This algorithm was devised by H. R. Glahn (personal communication) in 1967 and has been used for various applications by TDL and NMC. For instance, it is used for postprocessing the LFM forecasts (National Weather Service, 1974).

the sign of the two interpolated values agree, and the final value can be determined. Discrepancies exist in areas where the interpolations are of opposite signs. Where this happens, a value of zero is used.

A two-dimensional interpolation with actual data from a 1-h AS_d forecast is shown in Fig. 21. It shows an interpolation to a grid of 1/5 the original grid-length. The original gridpoints are shown as large crosses. The value on top of each point is from a biquadratic interpolation and the value underneath is from the procedure presented here. The dashed and solid lines illustrate the zero line from the biquadratic and specialized interpolations, respectively.

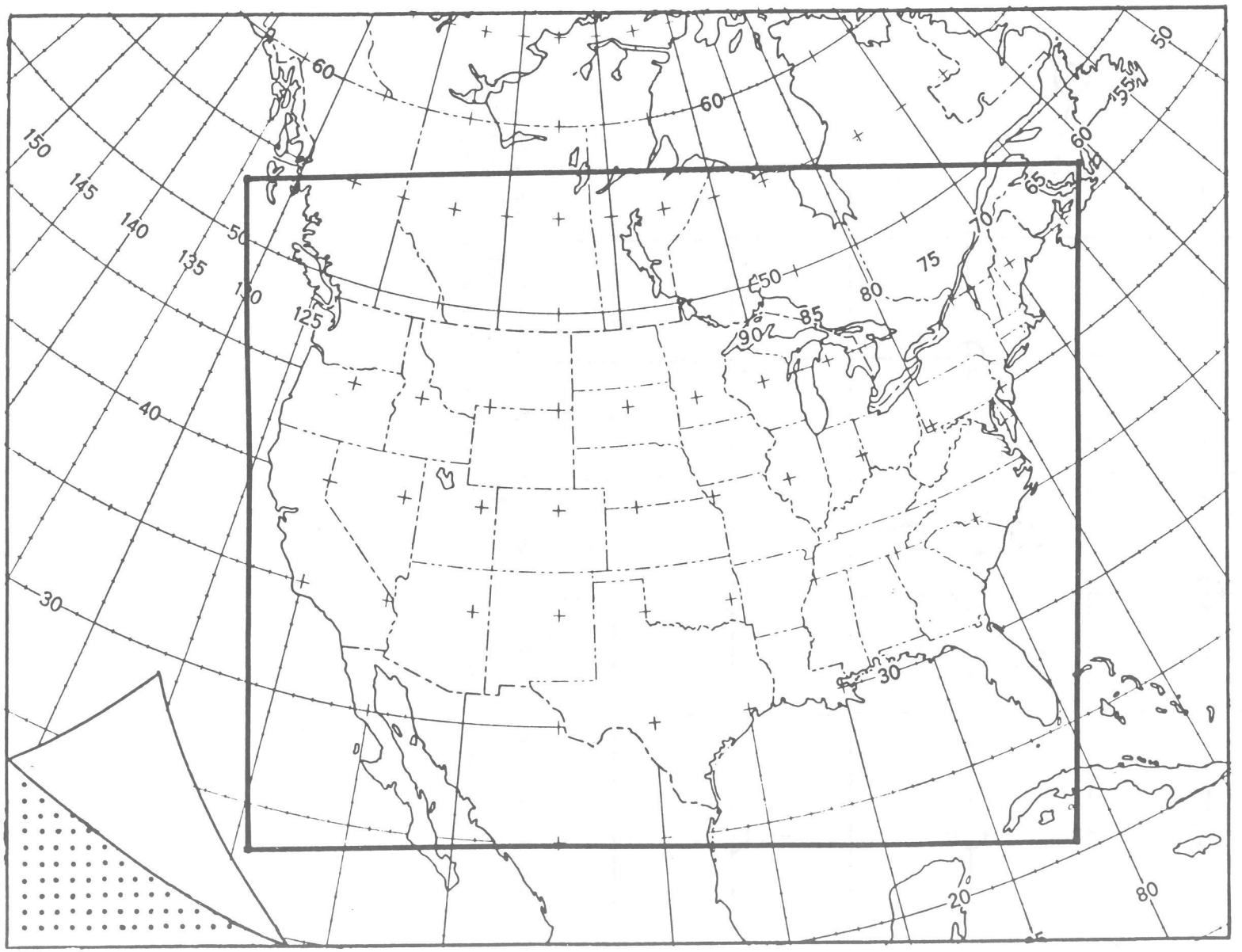

Figure 1. The area over which the moisture model is run. The grid spacing is shown in the lower left corner. The moisture model output is archived in the area within the inset rectangle.

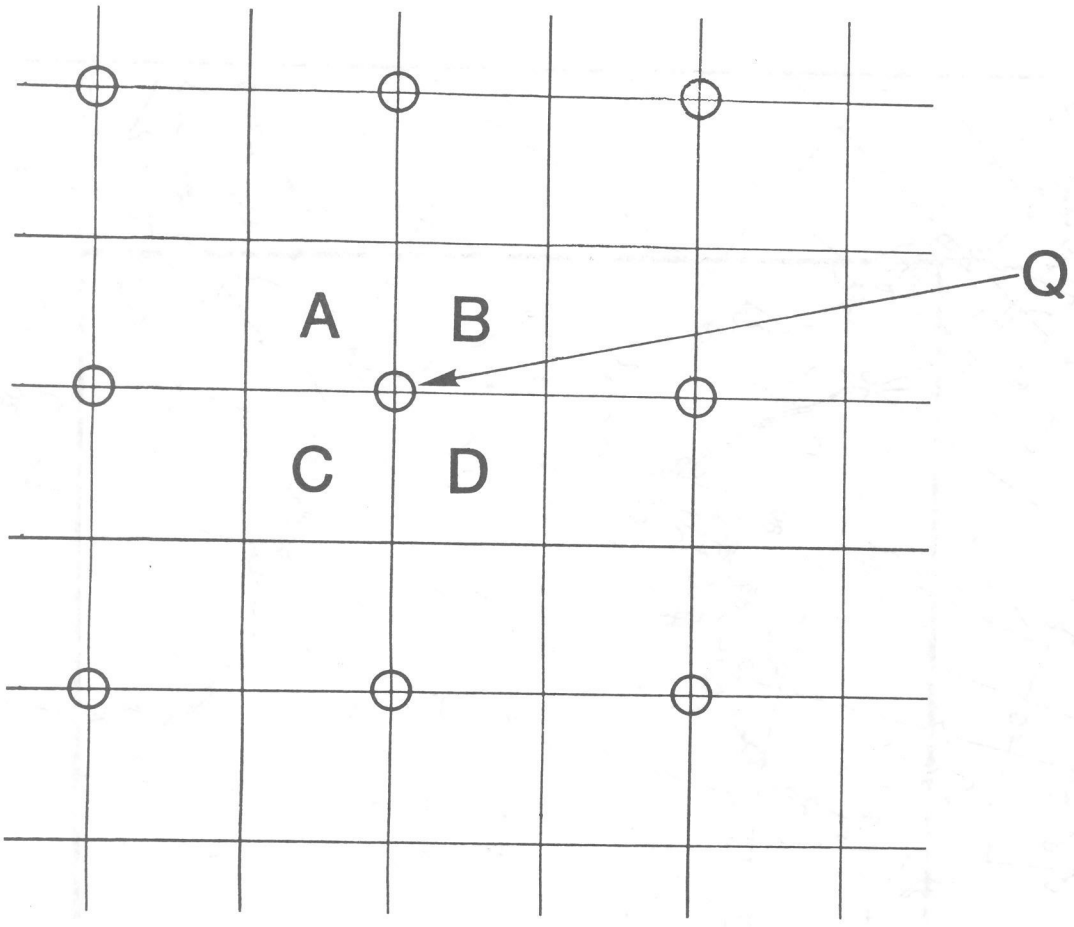

Figure 2. The relationship between LAMP gridpoints denoted by circles and MDR grid blocks. The MDR blocks labeled by letters are used to revise the S_d estimate at LAMP gridpoint Q.

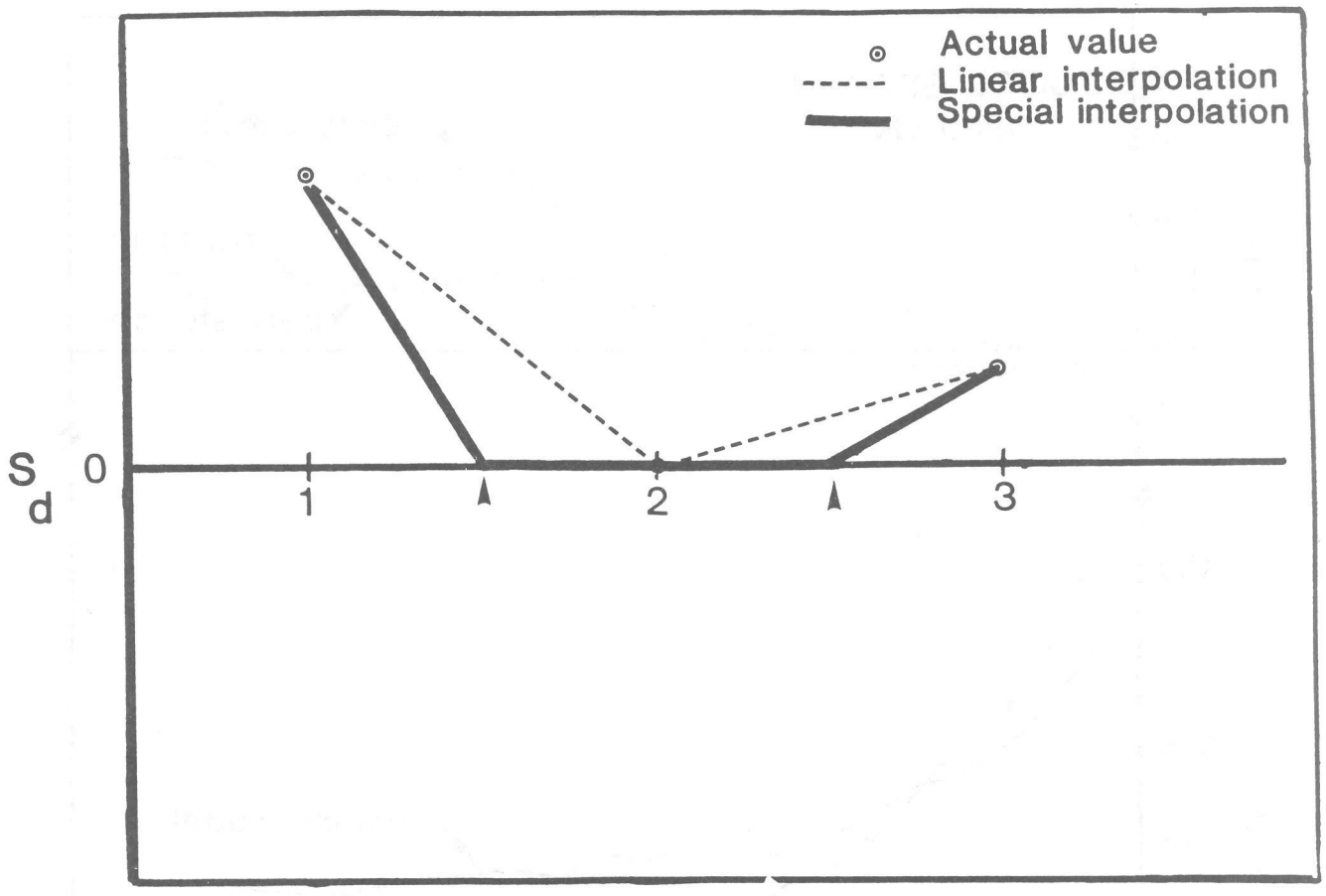

Figure 3. One dimensional illustration of placement of the zero line by a linear interpolation of a field S_d (broken line), and by the interpolation used in the moisture model (solid line). Precipitation would be represented at all points between the arrows for the moisture model interpolation.

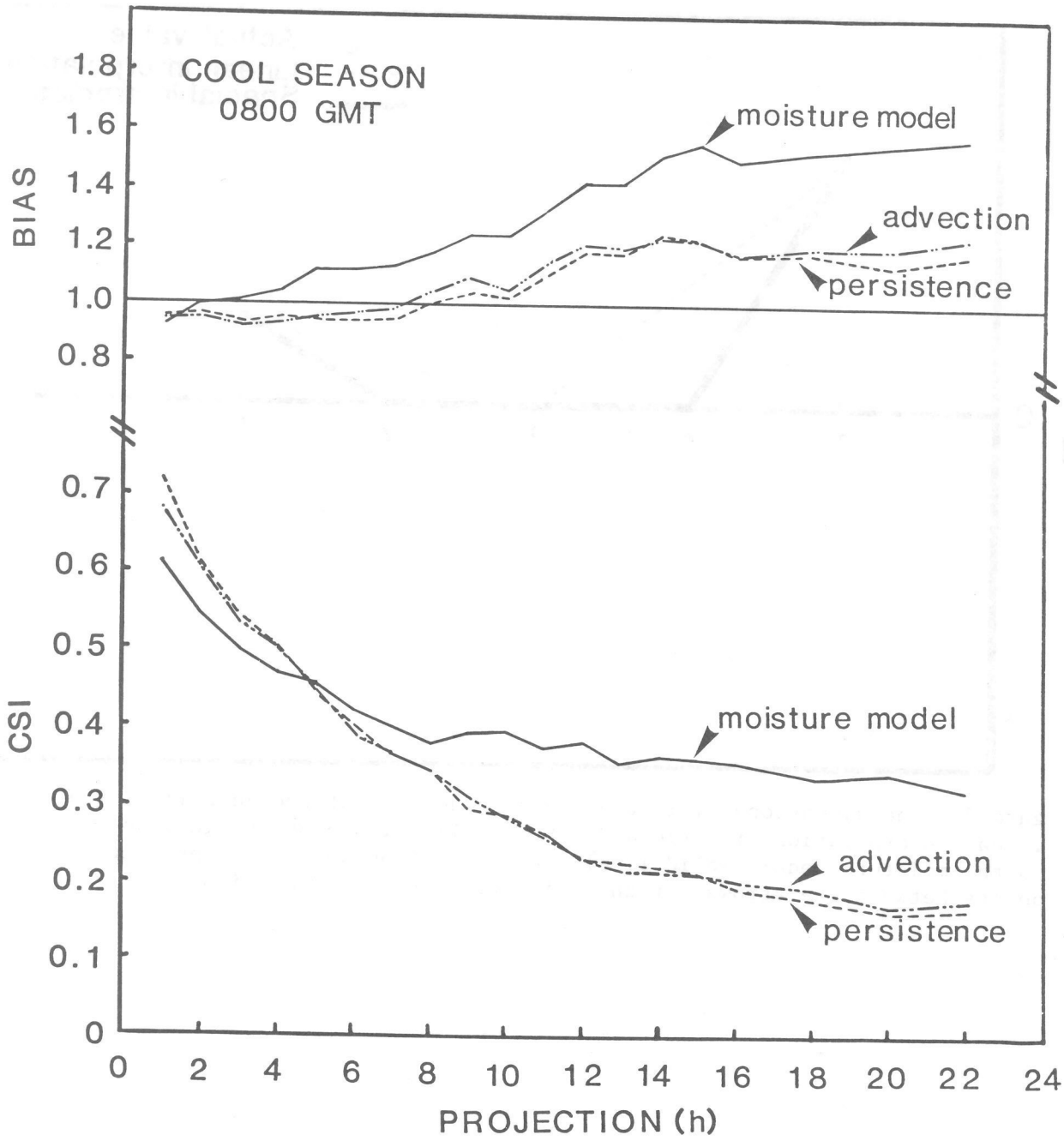

Figure 4. Critical success index and bias for 21 cool season predictions of instantaneous precipitation for projections from 1 through 22 hours. Scores for persistence, advection, and the moisture model from forecasts initialized at 0800 GMT are shown.

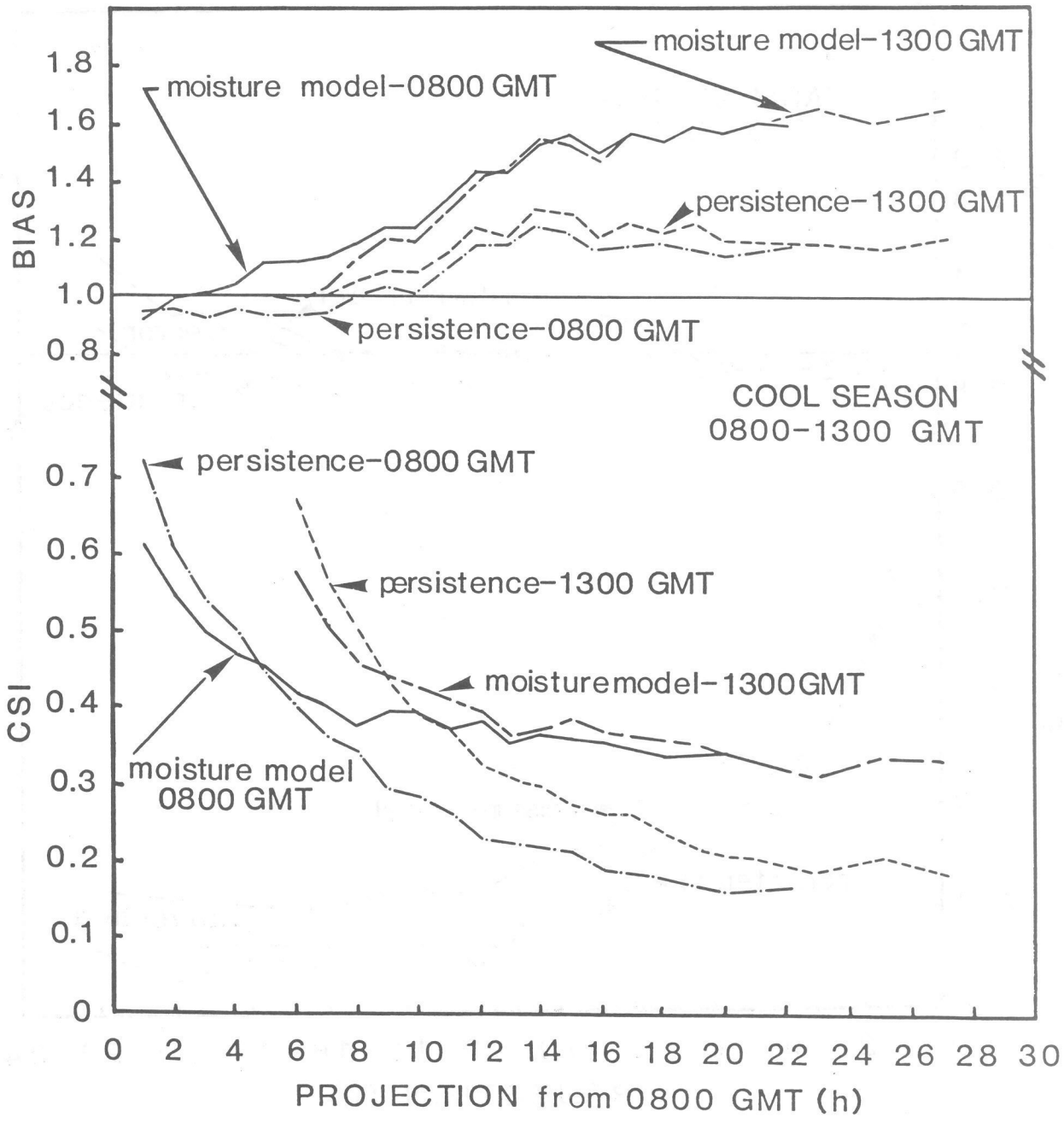

Figure 5. A comparison of the CSI and bias for cool season forecasts of instantaneous precipitation from forecasts initialized at 0800 and 1300 GMT. The projection hour shown is from the 0800 GMT model forecasts. The scores for 0800 GMT are identical to those from Fig. 4.

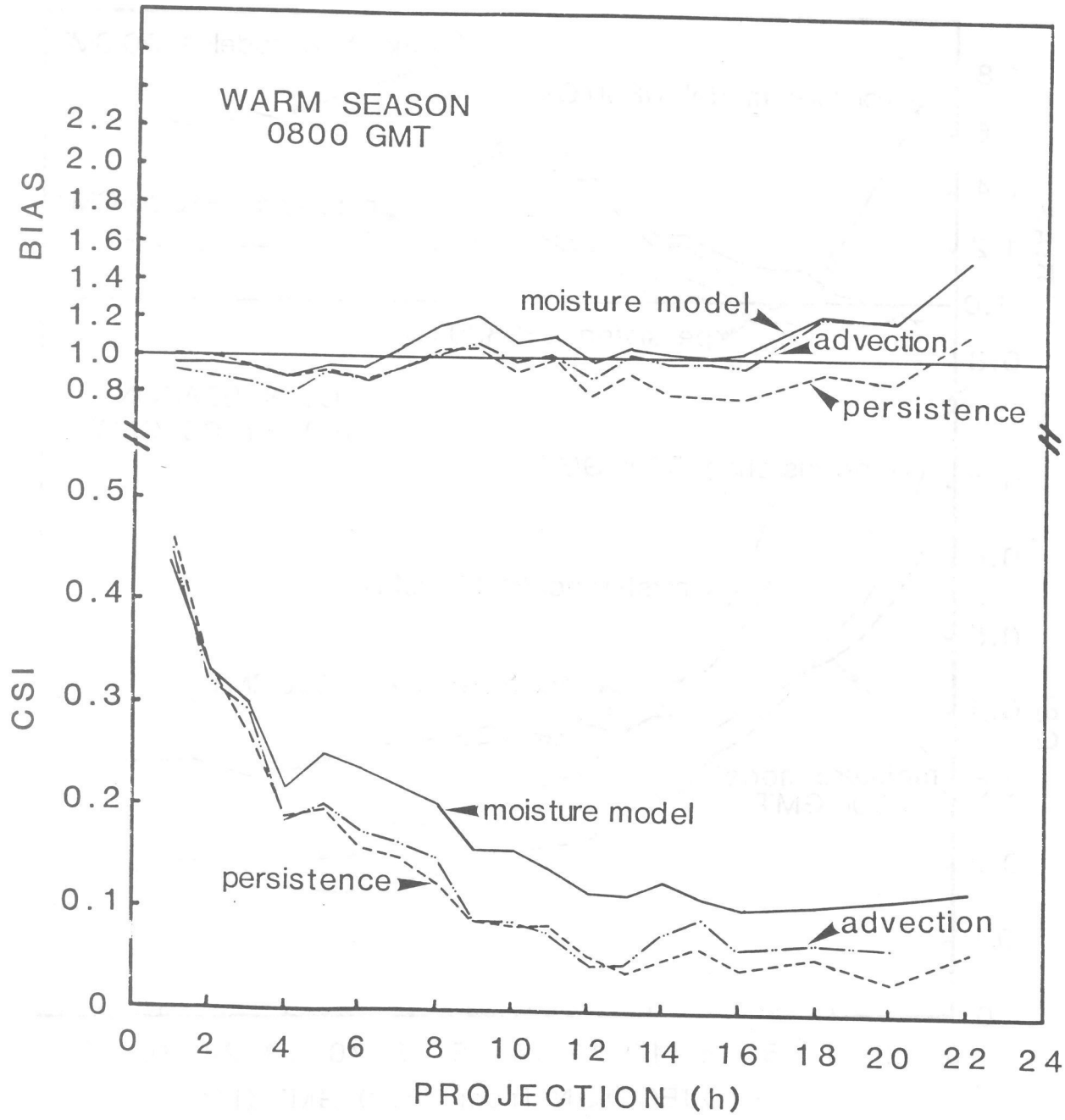

Figure 6. Same as Fig. 4 except for 21 warm season forecasts.

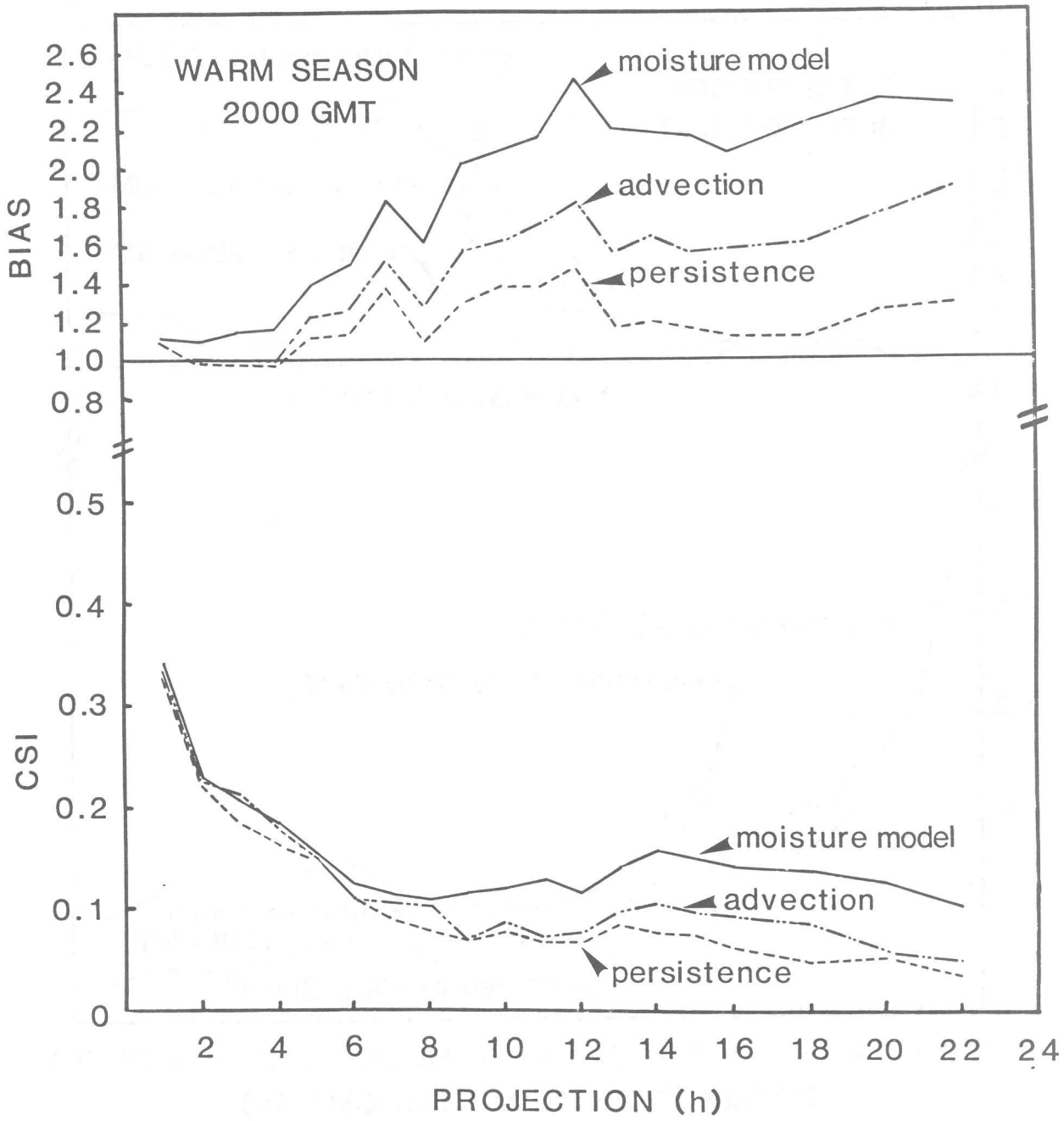

Figure 7. Same as Fig. 4 except for warm season forecasts initialized at 2000 GMT.

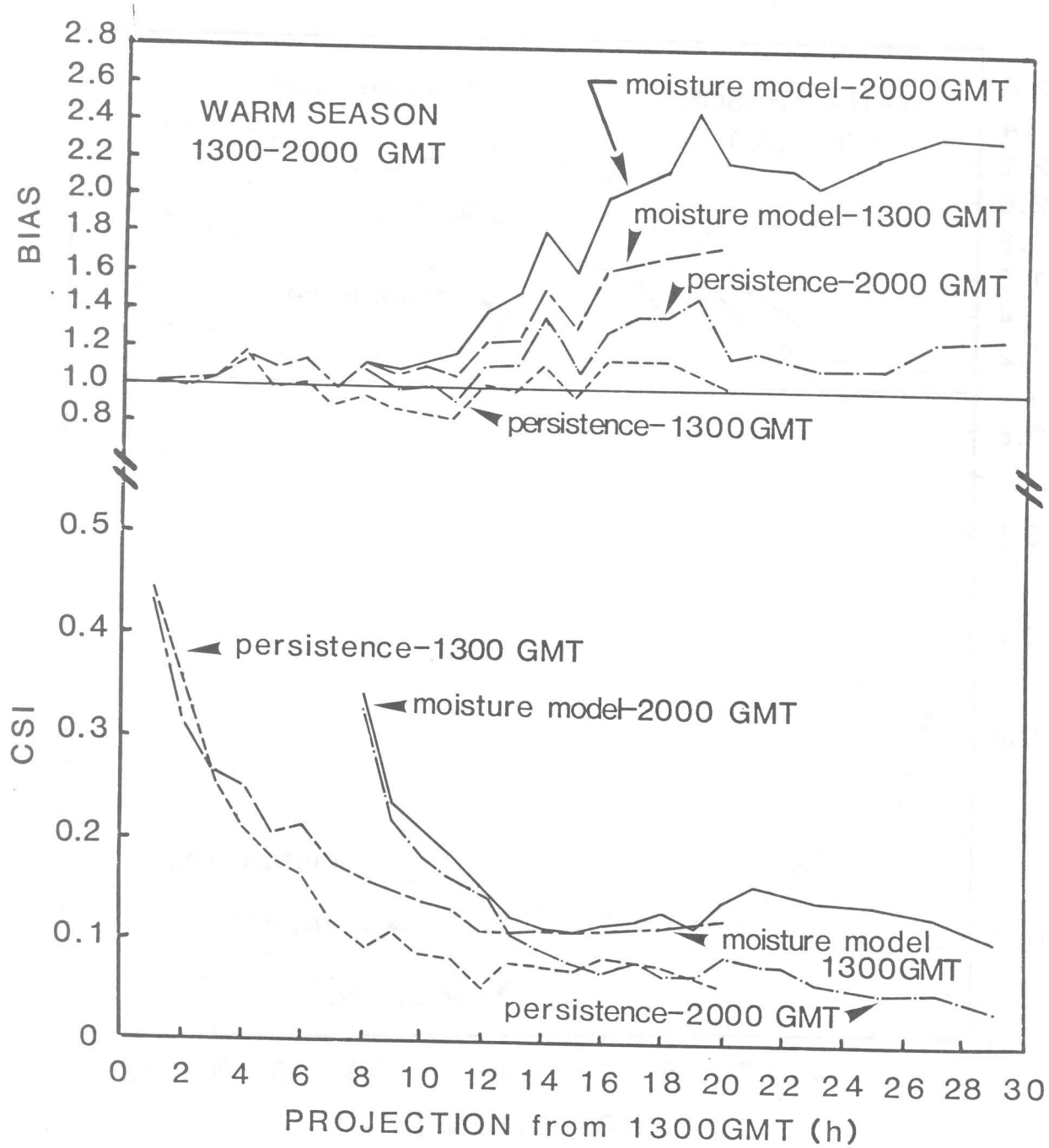

Figure 8. Same as Fig. 5 except for a comparison between warm season forecasts initialized at 1300 and 2000 GMT. Projections are from the 1300 GMT initialization time.

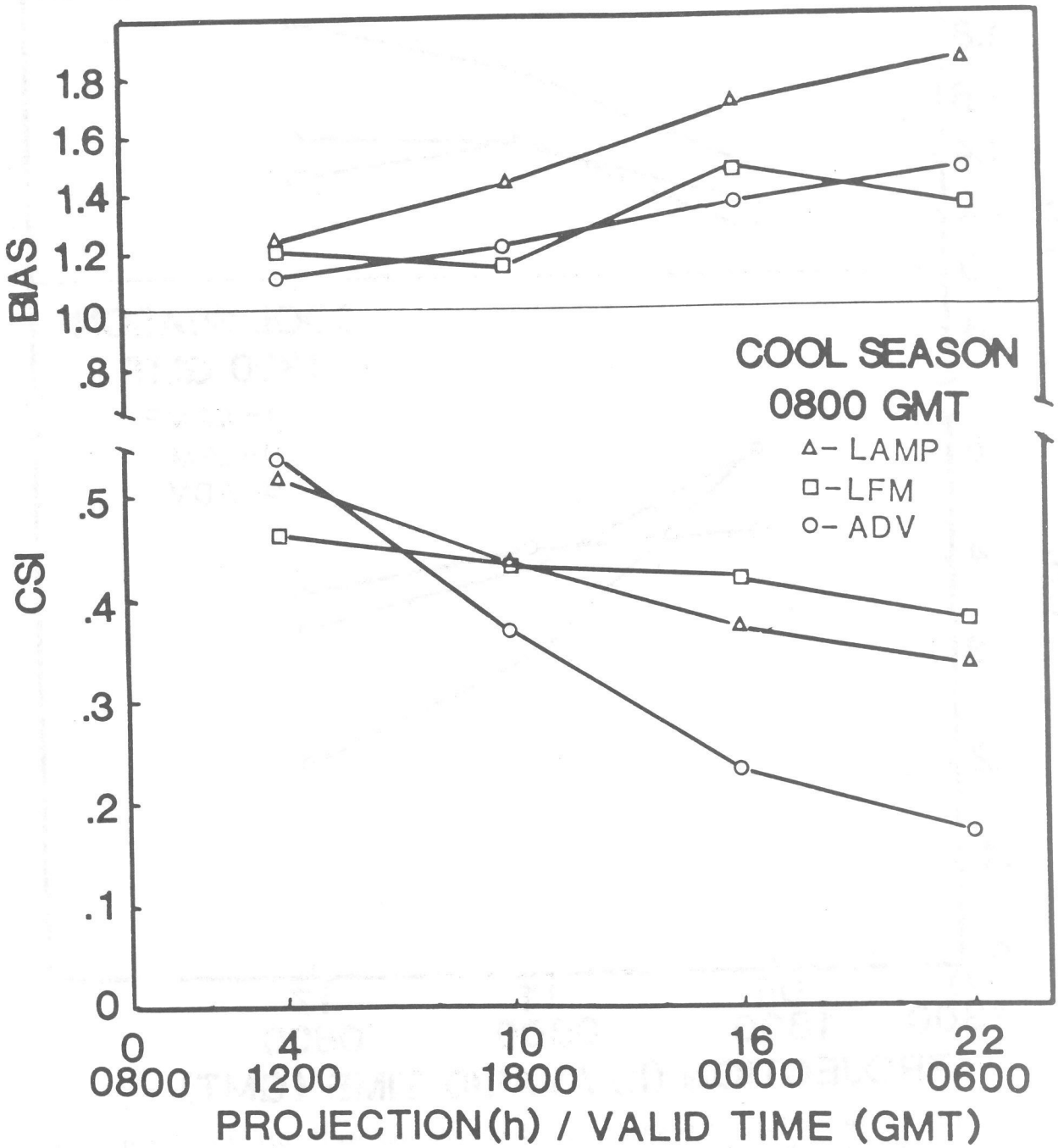

Figure 9. Critical success index and bias for cool season forecasts of measurable precipitation occurrence at stations for 6-h periods ending at the time shown. Scores for the LAMP and advection model are from models initialized at 0800 GMT; scores from the LFM model are from forecasts initialized at 0000 GMT.

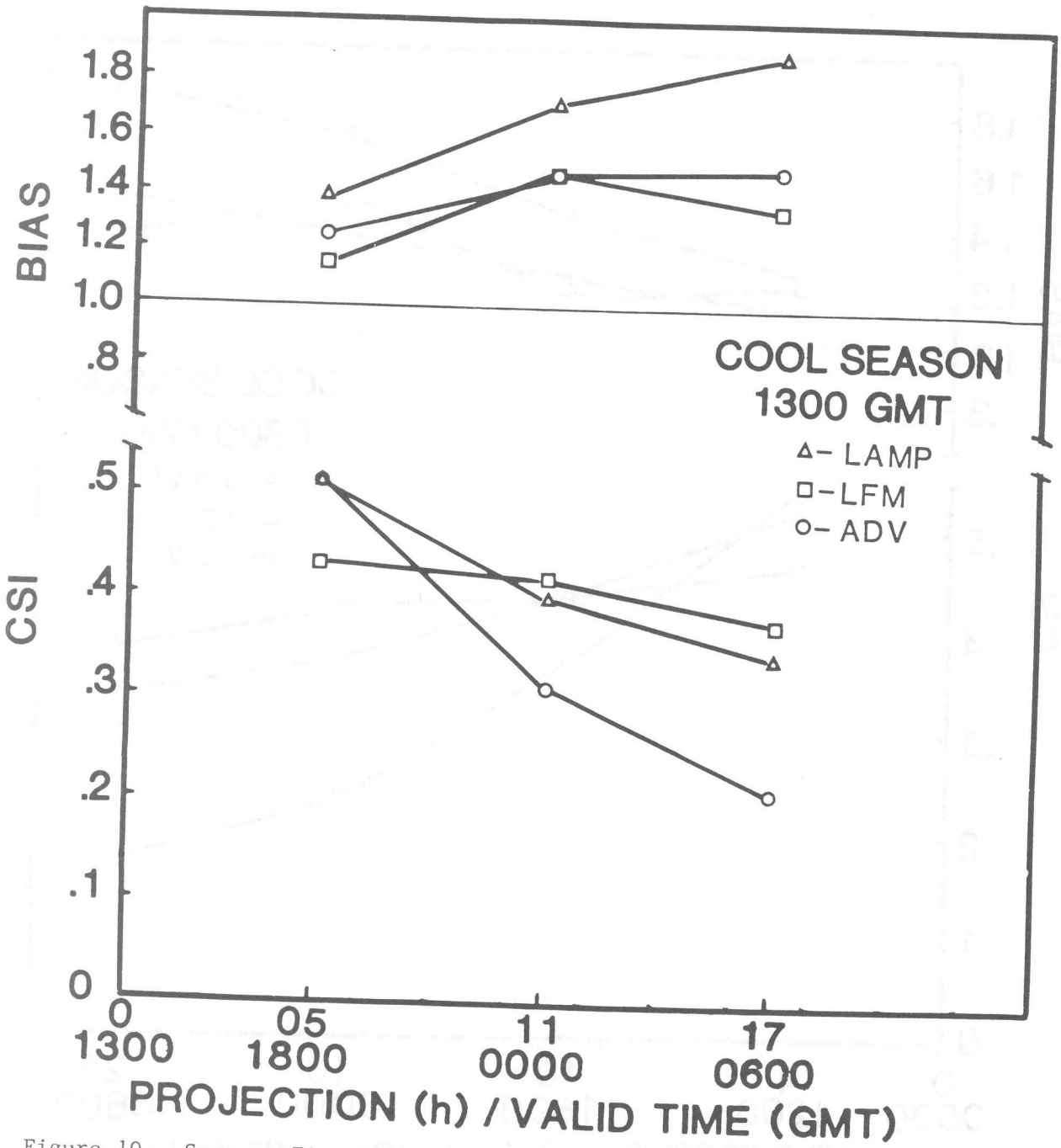

Figure 10. Same as Fig. 9 except for advection and moisture model forecasts initialized at 1300 GMT.

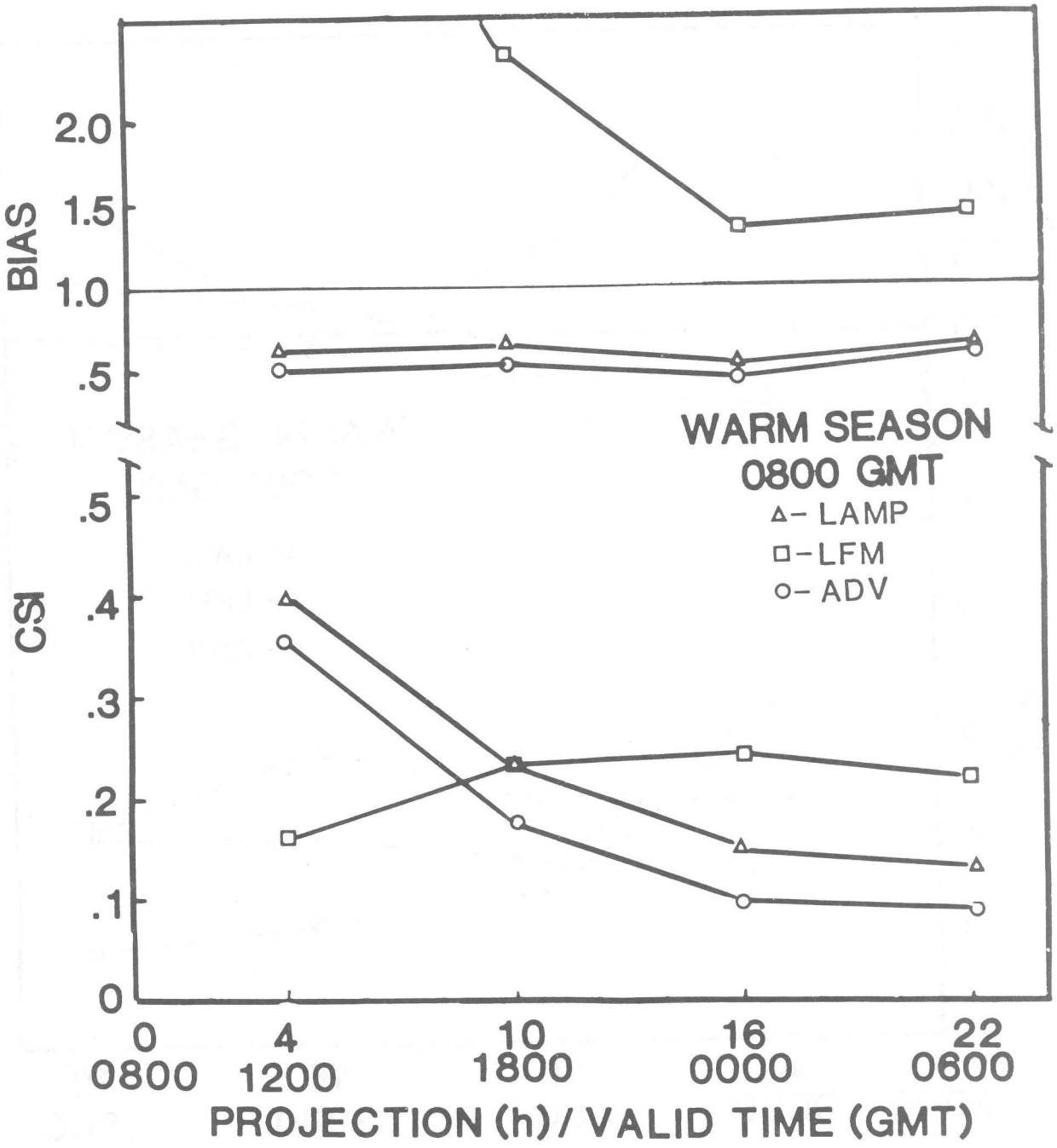

Figure 11. Same as Fig. 9 except for warm season forecasts.

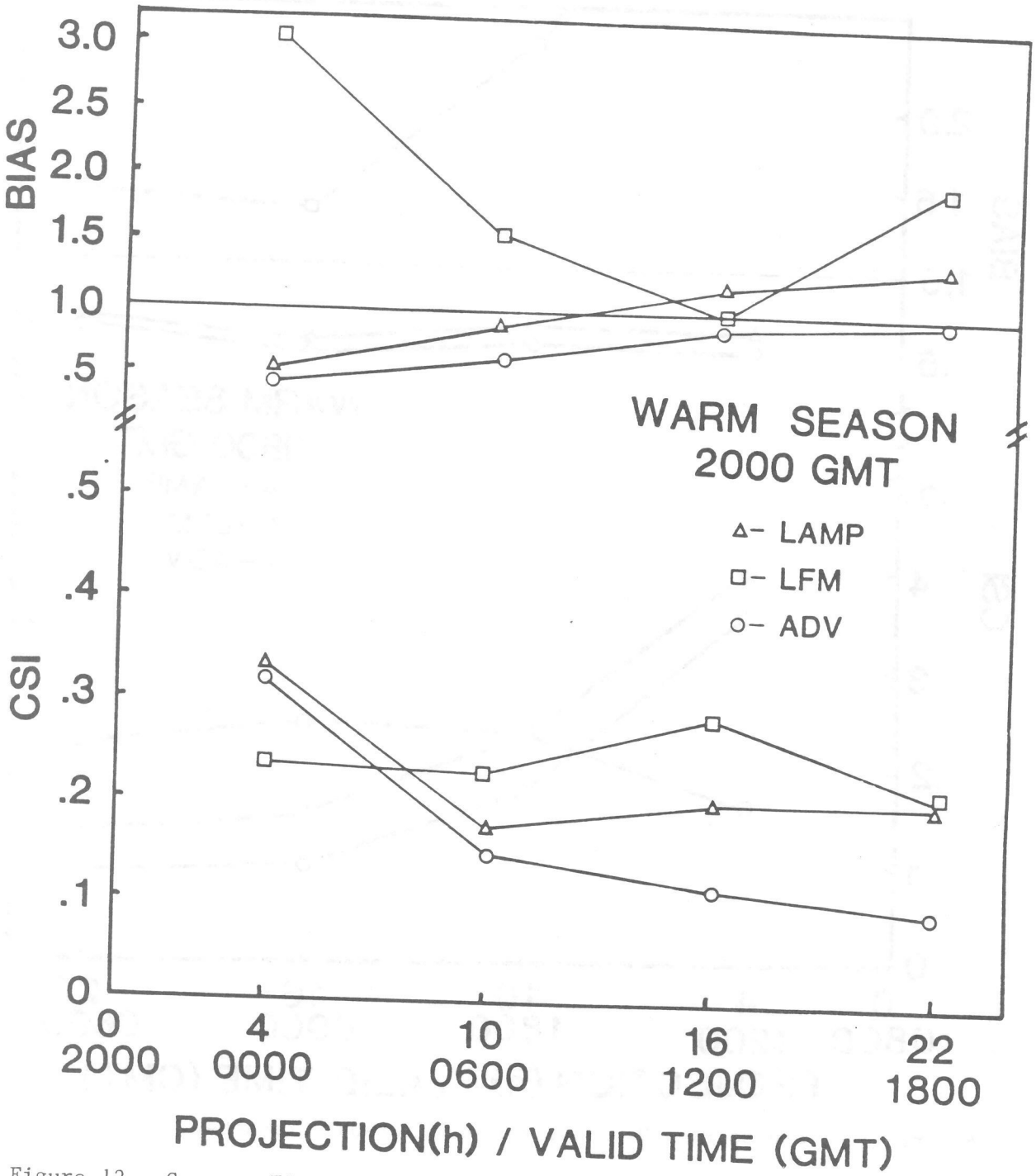

Figure 12. Same as Fig. 9 except for warm season forecasts initialized at 2000 GMT for the moisture and advection models, and at 1200 GMT for the LFM.

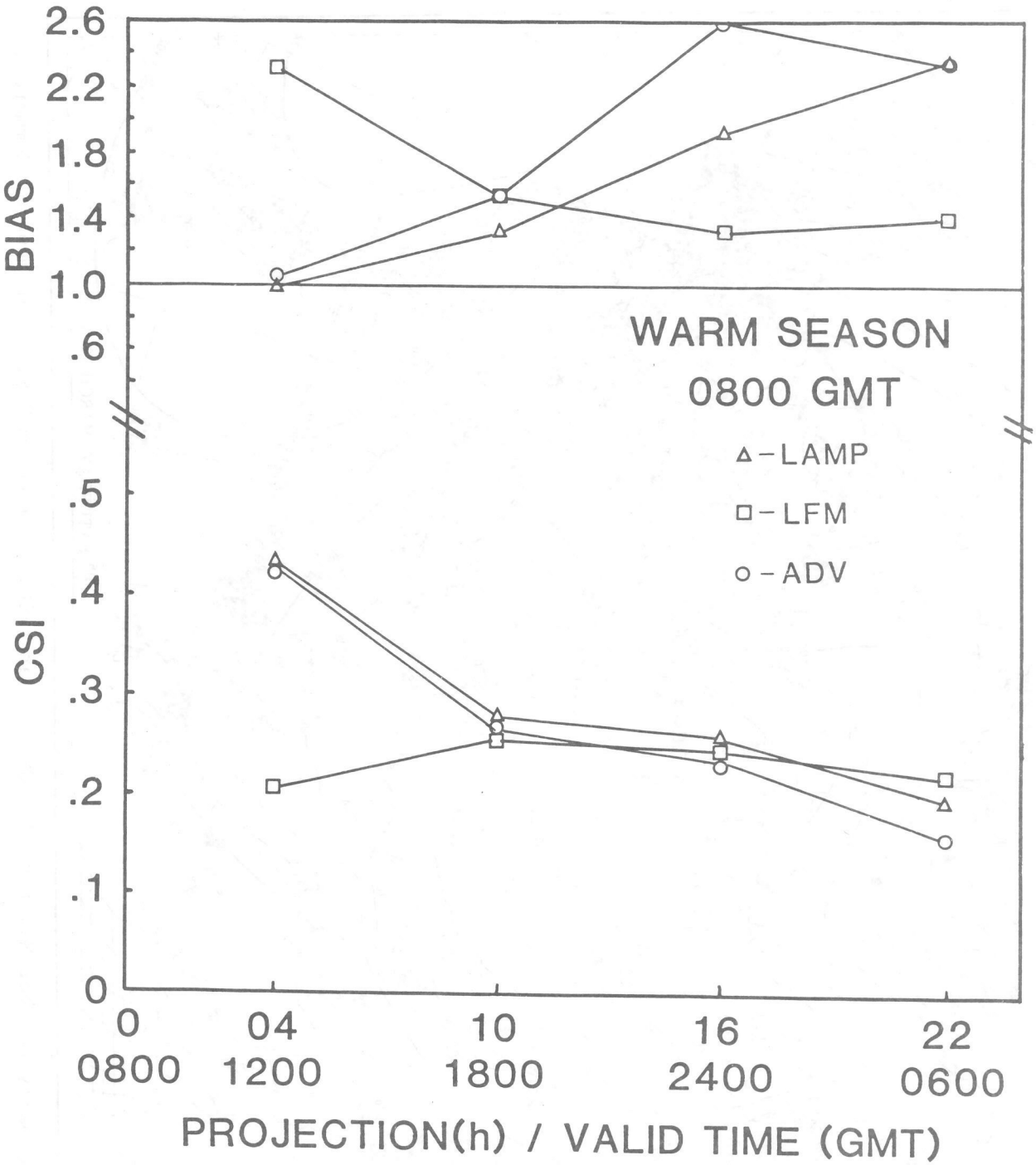

Figure 13. Same as Fig. 9 except for warm season forecasts in which the predictions have been adjusted to maximize the CSI score.

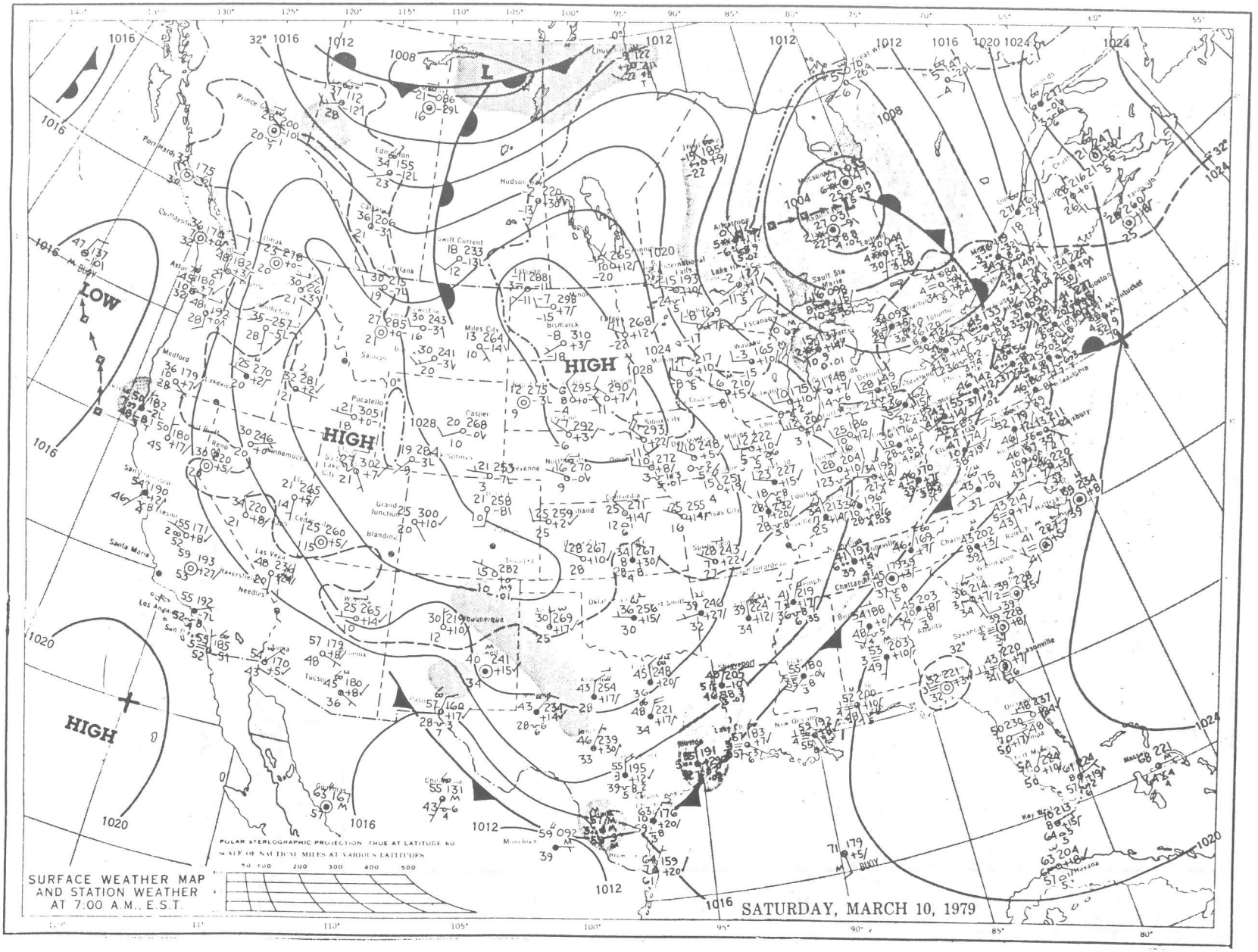

Figure 14. The Daily Weather Map for 1200 GMT on March 10, 1979 (from U.S. Department of Commerce, 1979).

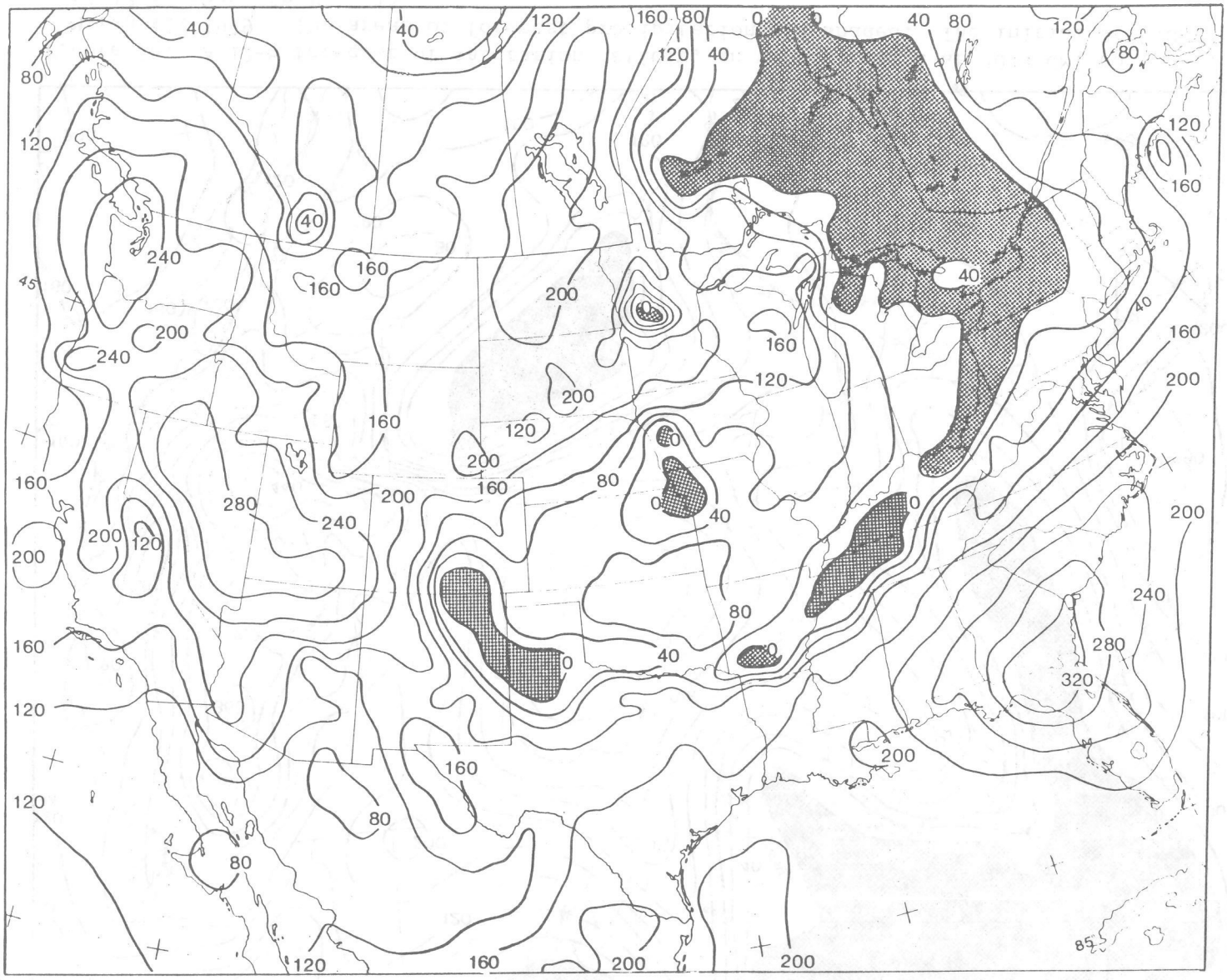

Figure 15. The saturation deficit analysis for 0800 GMT on March 10, 1979. Contours are in meters. The shaded area indicates where $S_d = 0$.

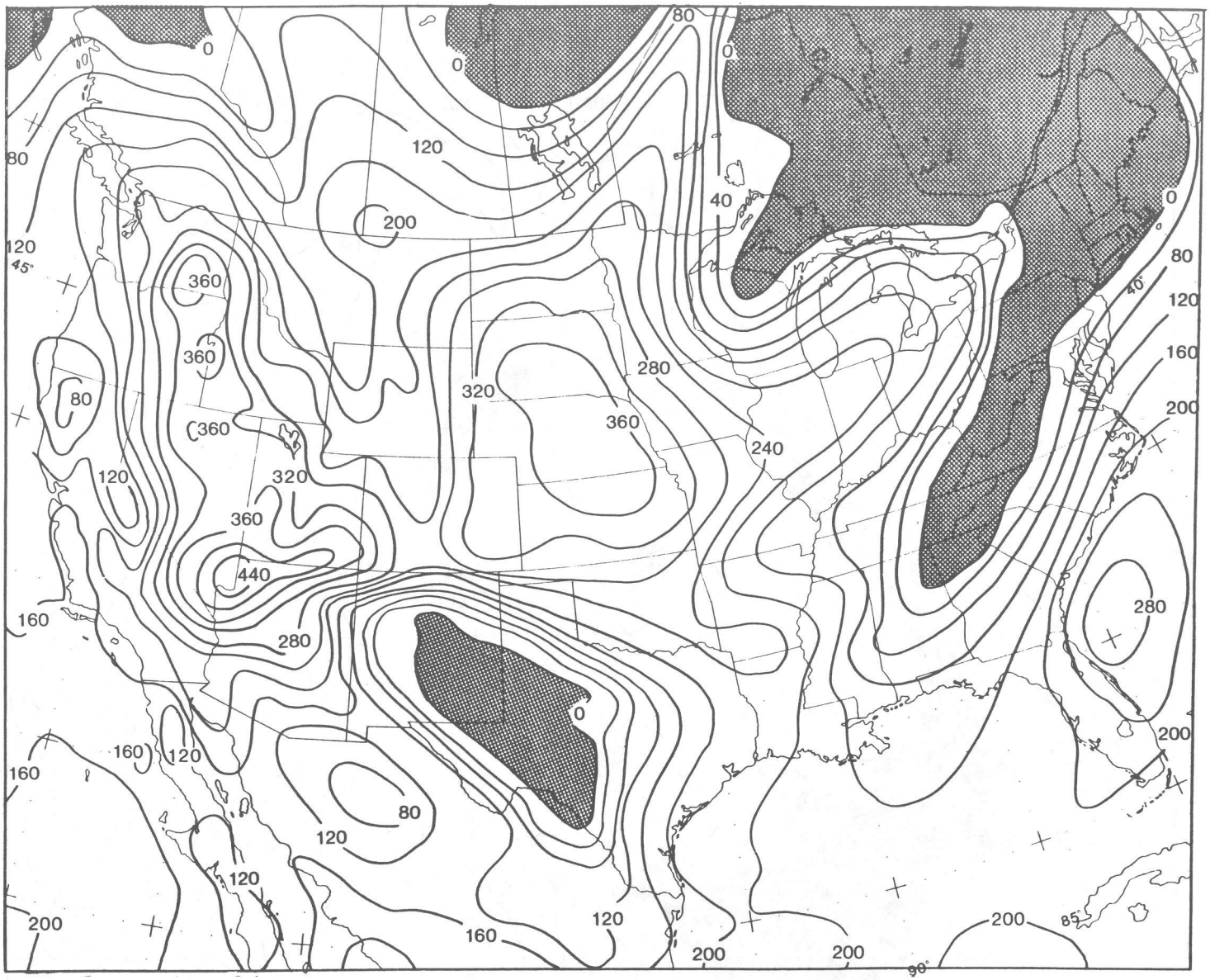

Figure 16. A 12-h forecast of saturation deficit, in meters, valid at 2000 GMT on March 10, 1979. The areas of forecast precipitation are shaded. The initial 0800 GMT field is shown in Fig. 15

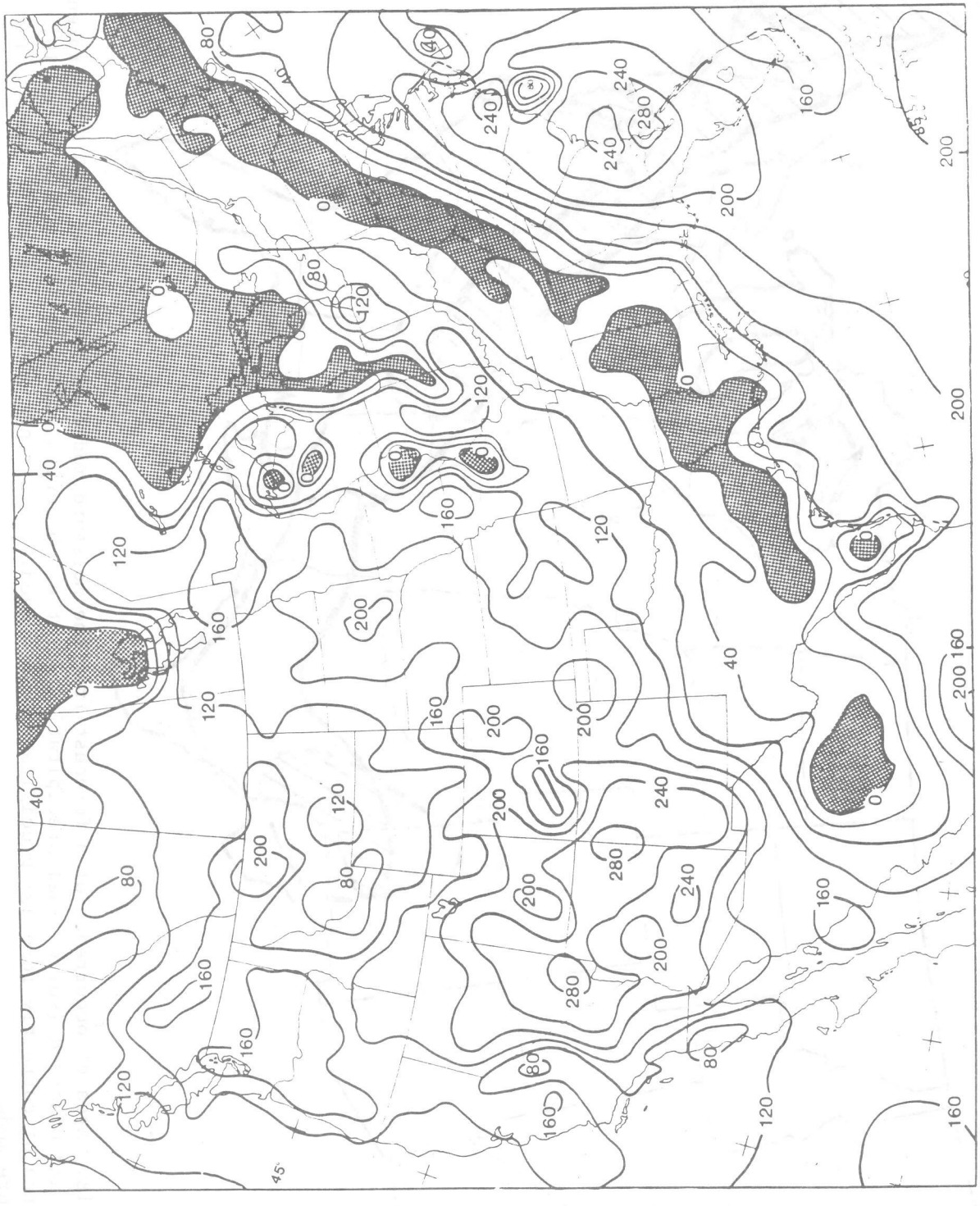

Figure 17. Same as Fig. 15 except for 2000 GMT.

Figure 18. Area of occurrence of a forecast from the moisture model initialized at 0800 GMT (broken line) and observed (solid line) precipitation for the 6-h period ending at 1800 GMT on March 10, 1979. The area of correctly forecast precipitation is shaded. This represents a 4 to 10 h forecast for the moisture model.

Figure 19. Same as Fig. 15 except for a 12- to 18-h forecast from the LFM model initialized at 0000 GMT.

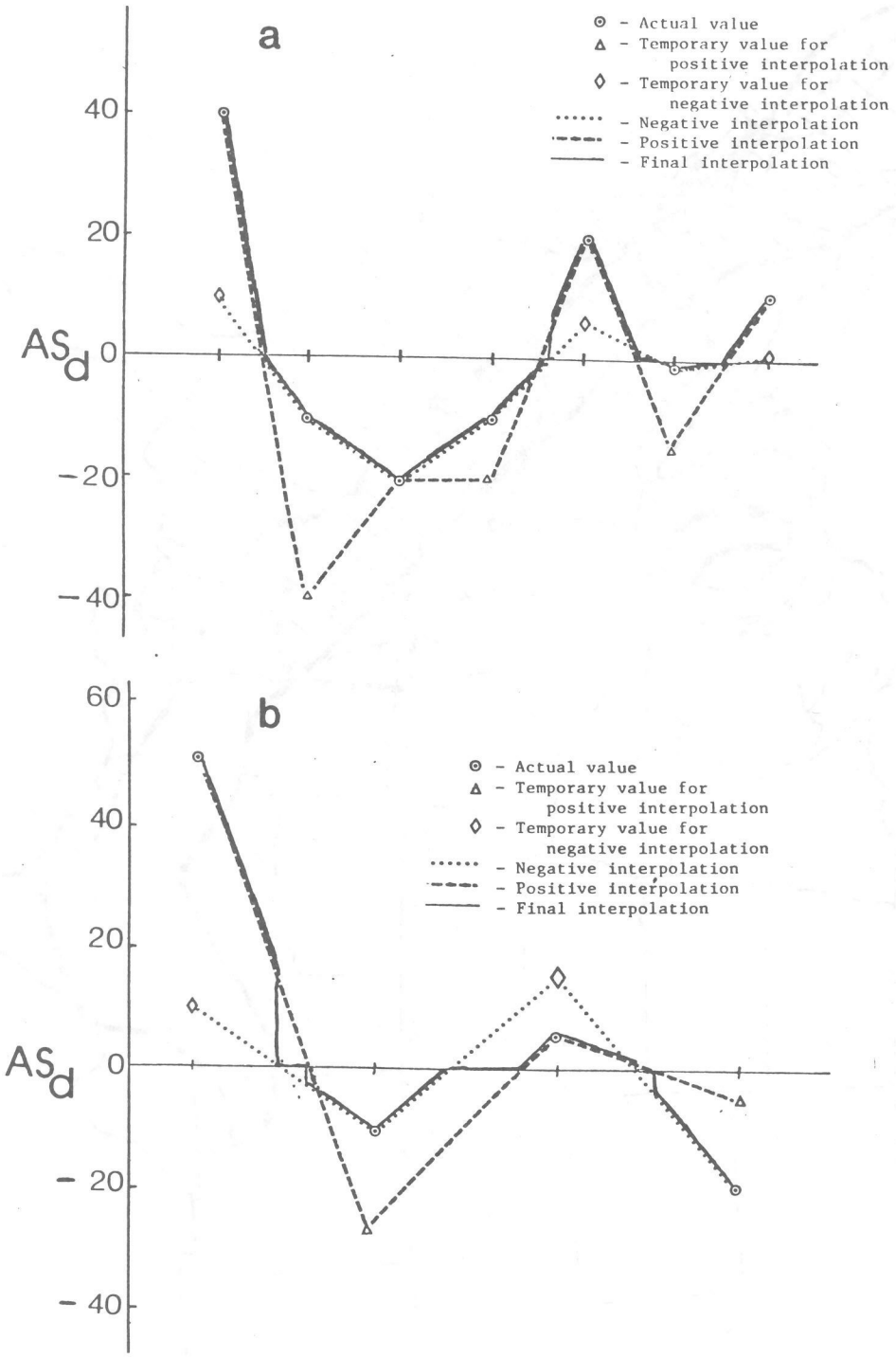

Figure 20. An example of an interpolation with the new routine is shown in 3a. The interpolations which are used to obtain positive values (dashed line), and negative values (dotted line) are shown along with the temporary values which were inserted at the gridpoints to obtain them. The final interpolation is shown by the solid line. Detail of a case in which there are discrepancies between the positive and negative interpolations is shown in 3b.

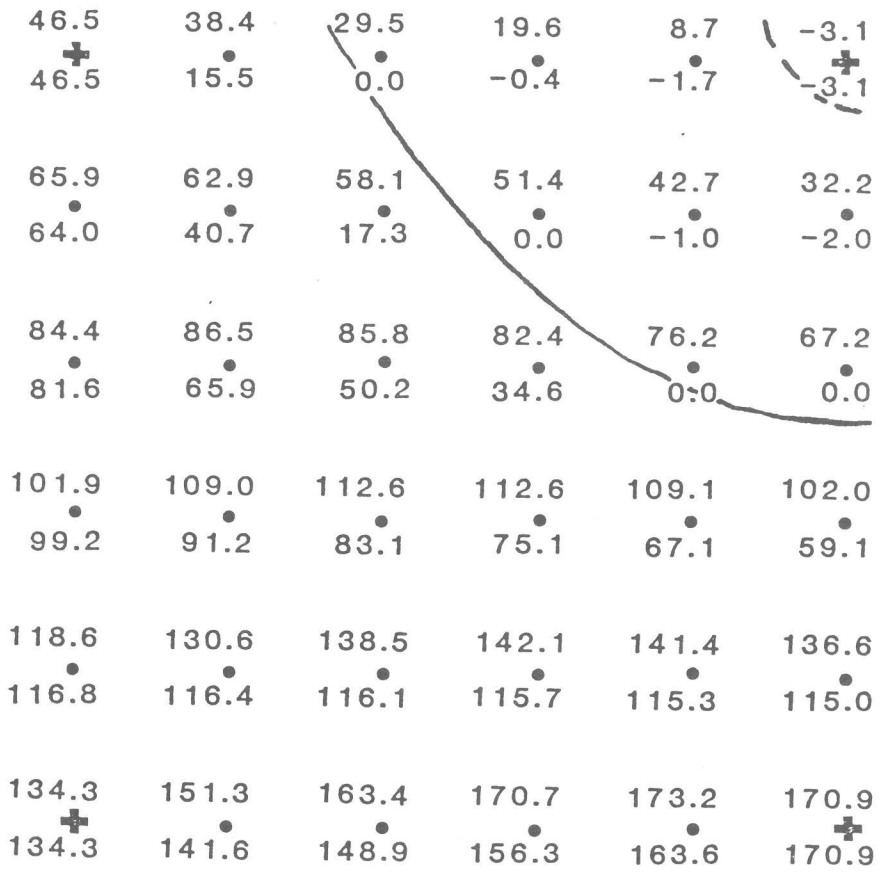

Figure 21. An example of a two-dimensional interpolation of data to a grid of one-fifth the original gridpoint spacing. The original data are shown at the crosses. The value from a biquadratic interpolation is shown above the point and the value from the new routine is shown below. The dashed curve shows the approximate zero line for the biquadratic interpolation, with that from the new interpolation shown by the solid curve.

(Continued from inside front cover)

NOAA Technical Memorandums

NWS TDL 42 Some Experiments With a Fine-Mesh 500-Millibar Barotropic Model. Robert J. Bermowitz, August 1971, 20 pp. (COM-71-00958)

NWS TDL 43 Air-Sea Energy Exchange in Lagrangian Temperature and Dew Point Forecasts. Ronald M. Reap, October 1971, 23 pp. (COM-71-01112)

NWS TDL 44 Use of Surface Observations in Boundary-Layer Analysis. H. Michael Mogil and William D. Bonner, March 1972, 16 pp. (COM-72-10641)

NWS TDL 45 The Use of Model Output Statistics (MOS) To Estimate Daily Maximum Temperatures. John R. Annett, Harry R. Glahn, and Dale A. Lowry, March 1972, 14 pp. (COM-72-10753)

NWS TDL 46 SPLASH (Special Program to List Amplitudes of Surges From Hurricanes): I. Landfall Storms. Chester P. Jelesnianski, April 1972, 52 pp. (COM-72-10807)

NWS TDL 47 Mean Diurnal and Monthly Height Changes in the Troposphere Over North America and Vicinity. August F. Korte and DeVer Colson, August 1972, 30 pp. (COM-72-11132)

NWS TDL 48 Synoptic Climatological Studies of Precipitation in the Plateau States From 850-, 700-, and 500-Millibar Lows During Spring. August F. Korte, Donald L. Jorgensen, and William H. Klein, August 1972, 130 pp. (COM-73-10069)

NWS TDL 49 Synoptic Climatological Studies of Precipitation in the Plateau States From 850-Millibar Lows During Fall. August F. Korte and DeVer Colson, August 1972, 56 pp. (COM-74-10464)

NWS TDL 50 Forecasting Extratropical Storm Surges for the Northeast Coast of the United States. N. Arthur Pore, William S. Richardson, and Herman P. Perrotti, January 1974, 70 pp. (COM-74-10719)

NWS TDL 51 Predicting the Conditional Probability of Frozen Precipitation. Harry R. Glahn and Joseph R. Bocchieri, March 1974, 33 pp. (COM-74-10909)

NWS TDL 52 SPLASH (Special Program to List Amplitudes of Surges From Hurricanes): Part Two. General Track and Variant Storm Conditions. Chester P. Jelesnianski, March 1974, 55 pp. (COM-74-10925)

NWS TDL 53 A Comparison Between the Single Station and Generalized Operator Techniques for Automated Prediction of Precipitation Probability. Joseph R. Bocchieri, September 1974, 20 pp. (COM-74-11763)

NWS TDL 54 Climatology of Lake Erie Storm Surges at Buffalo and Toledo. N. Arthur Pore, Herman P. Perrotti, and William S. Richardson, March 1975, 27 pp. (COM-75-10587)

NWS TDL 55 Dissipation, Dispersion and Difference Schemes. Paul E. Long, Jr., May 1975, 33 pp. (COM-75-10972)

NWS TDL 56 Some Physical and Numerical Aspects of Boundary Layer Modeling. Paul E. Long, Jr. and Wilson A. Shaffer, May 1975, 37 pp. (COM-75-10980)

NWS TDL 57 A Predictive Boundary Layer Model. Wilson A. Shaffer and Paul E. Long, Jr., May 1975, 44 pp. (PB-265-412)

NWS TDL 58 A Preliminary View of Storm Surges Before and after Storm Modifications for Alongshore-Moving Storms. Chester P. Jelesnianski and Celso S. Barrientos, October 1975, 16 pp. (PB-247-362)

NWS TDL 59 Assimilation of Surface, Upper Air, and Grid-Point Data in the Objective Analysis Procedure for a Three-Dimensional Trajectory Model. Ronald M. Reap, February 1976, 17 pp. (PB-256-082)

NWS TDL 60 Verification of Severe Local Storms Warnings Based on Radar Echo Characteristics. Donald S. Foster, June 1976, 9 pp. plus supplement. (PB-262-417)

NWS TDL 61 A Sheared Coordinate System for Storm Surge Equations of Motion With a Mildly Curved Coast. Chester P. Jelesnianski, July 1976, 52 pp. (PB-261-956)

NWS TDL 62 Automated Prediction of Thunderstorms and Severe Local Storms. Ronald M. Reap and Donald S. Foster, April 1977, 20 pp. (PB-268-035)

NWS TDL 63 Automated Great Lakes Wave Forecasts. N. Arthur Pore, February 1977, 13 pp. (PB-265-854)

NWS TDL 64 Operational System for Predicting Thunderstorms Two to Six Hours in Advance. Jerome P. Charba, March 1977, 24 pp. (PB-266-969)

NWS TDL 65 Operational System for Predicting Severe Local Storms Two to Six Hours in Advance. Jerome P. Charba, May 1977, 36 pp. (PB-271-147)

NWS TDL 66 The State of the Techniques Development Laboratory's Boundary Layer Model: May 24, 1977. P. E. Long, W. A. Shaffer, J. E. Kemper, and F. J. Hicks, April 1978, 58 pp. (PB-287-821)

NWS TDL 67 Computer Worded Public Weather Forecasts. Harry R. Glahn, November 1978, 25 pp. (PB-291-517)

NWS TDL 68 A Simple Soil Heat Flux Calculation for Numerical Models. Wilson A. Shaffer, May 1979, 16 pp. (PB-297-350)

NWS TDL 69 Comparison and Verification of Dynamical and Statistical Lake Erie Storm Surge Forecasts. William S. Richardson and David J. Schwab, November 1979, 20 pp. (PB80 137797)

NWS TDL 70 The Sea Level Pressure Prediction Model of the Local AFOS MOS Program. David A. Unger, April 1982, 33 pp. (PB82 215492)

NWS TDL 71 A Tide Climatology for Boston, Massachusetts. William S. Richardson, N. Arthur Pore, and David M. Feit, November 1982, 67 pp. (PB83 144196)

NWS TDL 72 Experimental Wind Forecasts From the Local AFOS MOS Program. Harry R. Glahn, January 1984, 60 pp. (PB84-155514)

NWS TDL 73 Trends in Skill and Accuracy of National Weather Service POP Forecasts. Harry R. Glahn, July 1984, 34 pp. (PB84 229053)

NWS TDL 74 Great Lakes Nearshore Wind Predictions from Great Lakes MOS Wind Guidance. Lawrence D. Burroughs, July 1984, 21 pp. (PB85 212876/AS)

NWS TDL 75 Objective Map Analysis for the Local AFOS MOS Program. Harry R. Glahn, Timothy L. Chambers, William S. Richardson, and Herman P. Perrotti, March 1985, 35 pp. (PB85 212884/AS)

NWS TDL 76 The Application of Cumulus Models to MOS Forecasts of Convective Weather. David H. Kitzmiller, June 1985, 50 pp. (PB86 1366867AS)

(Continued from inside front cover)

NOAA Technical Memorandums

NWS TDL 42 Some Experiments With a Fine-Mesh 500-Millibar Barotropic Model. Robert J. Bermowitz, August 1971, 20 pp. (COM-71-00958)

NWS TDL 43 Air-Sea Energy Exchange in Lagrangian Temperature and Dew Point Forecasts. Ronald M. Reap, October 1971, 23 pp. (COM-71-01112)

NWS TDL 44 Use of Surface Observations in Boundary-Layer Analysis. H. Michael Mogil and William D. Bonner, March 1972, 16 pp. (COM-72-10641)

NWS TDL 45 The Use of Model Output Statistics (MOS) To Estimate Daily Maximum Temperatures. John R. Annett, Harry R. Glahn, and Dale A. Lowry, March 1972, 14 pp. (COM-72-10753)

NWS TDL 46 SPLASH (Special Program to List Amplitudes of Surges From Hurricanes): I. Landfall Storms. Chester P. Jelesnianski, April 1972, 52 pp. (COM-72-10807)

NWS TDL 47 Mean Diurnal and Monthly Height Changes in the Troposphere Over North America and Vicinity. August F. Korte and DeVer Colson, August 1972, 30 pp. (COM-72-11132)

NWS TDL 48 Synoptic Climatological Studies of Precipitation in the Plateau States From 850-, 700-, and 500-Millibar Lows During Spring. August F. Korte, Donald L. Jorgensen, and William H. Klein, August 1972, 130 pp. (COM-73-10069)

NWS TDL 49 Synoptic Climatological Studies of Precipitation in the Plateau States From 850-Millibar Lows During Fall. August F. Korte and DeVer Colson, August 1972, 56 pp. (COM-74-10464)

NWS TDL 50 Forecasting Extratropical Storm Surges for the Northeast Coast of the United States. N. Arthur Pore, William S. Richardson, and Herman P. Perrotti, January 1974, 70 pp. (COM-74-10719)

NWS TDL 51 Predicting the Conditional Probability of Frozen Precipitation. Harry R. Glahn and Joseph R. Bocchieri, March 1974, 33 pp. (COM-74-10909)

NWS TDL 52 SPLASH (Special Program to List Amplitudes of Surges From Hurricanes): Part Two. General Track and Variant Storm Conditions. Chester P. Jelesnianski, March 1974, 55 pp. (COM-74-10925)

NWS TDL 53 A Comparison Between the Single Station and Generalized Operator Techniques for Automated Prediction of Precipitation Probability. Joseph R. Bocchieri, September 1974, 20 pp. (COM-74-11763)

NWS TDL 54 Climatology of Lake Erie Storm Surges at Buffalo and Toledo. N. Arthur Pore, Herman P. Perrotti, and William S. Richardson, March 1975, 27 pp. (COM-75-10587)

NWS TDL 55 Dissipation, Dispersion and Difference Schemes. Paul E. Long, Jr., May 1975, 33 pp. (COM-75-10972)

NWS TDL 56 Some Physical and Numerical Aspects of Boundary Layer Modeling. Paul E. Long, Jr. and Wilson A. Shaffer, May 1975, 37 pp. (COM-75-10980)

NWS TDL 57 A Predictive Boundary Layer Model. Wilson A. Shaffer and Paul E. Long, Jr., May 1975, 44 pp. (PB-265-412)

NWS TDL 58 A Preliminary View of Storm Surges Before and after Storm Modifications for Alongshore-Moving Storms. Chester P. Jelesnianski and Celso S. Barrientos, October 1975, 16 pp. (PB-247-362)

NWS TDL 59 Assimilation of Surface, Upper Air, and Grid-Point Data in the Objective Analysis Procedure for a Three-Dimensional Trajectory Model. Ronald M. Reap, February 1976, 17 pp. (PB-256-082)

NWS TDL 60 Verification of Severe Local Storms Warnings Based on Radar Echo Characteristics. Donald S. Foster, June 1976, 9 pp. plus supplement. (PB-262-417)

NWS TDL 61 A Sheared Coordinate System for Storm Surge Equations of Motion With a Mildly Curved Coast. Chester P. Jelesnianski, July 1976, 52 pp. (PB-261-956)

NWS TDL 62 Automated Prediction of Thunderstorms and Severe Local Storms. Ronald M. Reap and Donald S. Foster, April 1977, 20 pp. (PB-268-035)

NWS TDL 63 Automated Great Lakes Wave Forecasts. N. Arthur Pore, February 1977, 13 pp. (PB-265-854)

NWS TDL 64 Operational System for Predicting Thunderstorms Two to Six Hours in Advance. Jerome P. Charba, March 1977, 24 pp. (PB-266-969)

NWS TDL 65 Operational System for Predicting Severe Local Storms Two to Six Hours in Advance. Jerome P. Charba, May 1977, 36 pp. (PB-271-147)

NWS TDL 66 The State of the Techniques Development Laboratory's Boundary Layer Model: May 24, 1977. P. E. Long, W. A. Shaffer, J. E. Kemper, and F. J. Hicks, April 1978, 58 pp. (PB-287-821)

NWS TDL 67 Computer Worded Public Weather Forecasts. Harry R. Glahn, November 1978, 25 pp. (PB-291-517)

NWS TDL 68 A Simple Soil Heat Flux Calculation for Numerical Models. Wilson A. Shaffer, May 1979, 16 pp. (PB-297-350)

NWS TDL 69 Comparison and Verification of Dynamical and Statistical Lake Erie Storm Surge Forecasts. William S. Richardson and David J. Schwab, November 1979, 20 pp. (PB80 137797)

NWS TDL 70 The Sea Level Pressure Prediction Model of the Local AFOS MOS Program. David A. Unger, April 1982, 33 pp. (PB82 215492)

NWS TDL 71 A Tide Climatology for Boston, Massachusetts. William S. Richardson, N. Arthur Pore, and David M. Feit, November 1982, 67 pp. (PB83 144196)

NWS TDL 72 Experimental Wind Forecasts From the Local AFOS MOS Program. Harry R. Glahn, January 1984, 60 pp. (PB84-155514)

NWS TDL 73 Trends in Skill and Accuracy of National Weather Service POP Forecasts. Harry R. Glahn, July 1984, 34 pp. (PB84 229053)

NWS TDL 74 Great Lakes Nearshore Wind Predictions from Great Lakes MOS Wind Guidance. Lawrence D. Burroughs, July 1984, 21 pp. (PB85 212876/AS)

NWS TDL 75 Objective Map Analysis for the Local AFOS MOS Program. Harry R. Glahn, Timothy L. Chambers, William S. Richardson, and Herman P. Perrotti, March 1985, 35 pp. (PB85 212884/AS)

NWS TDL 76 The Application of Cumulus Models to MOS Forecasts of Convective Weather. David H. Kitzmiller, June 1985, 50 pp. (PB86 1366867AS)